Skeletal-Muscle Glutamine Synthase is Upregulated in Preclinical Prion Diseases

Davide Caredio*[1], Maruša Koderman*[1], Karl Frontzek[1,2,3], Silvia Sorce[1], Mario Nuvolone[1,4], Juliane Bremer[1,5], Petra Schwarz[1], Stefano Sellitto[1], Nathalie Streichenberger[6], Claudia Scheckel[1], Adriano Aguzzi✉[1]

[1] Institute of Neuropathology, University Hospital Zurich, University of Zurich, Schmelzbergstrasse 12, CH-8091 Zurich, Switzerland.

[2] Department of Molecular Neuroscience, Weizmann Institute of Science, Rehovot, Israel.

[3] Current affiliation: Queen Square Brain Bank, University College of London Queen Square Institute of Neurology, London, England

[4] Current affiliation: Amyloidosis Research and Treatment Center, Fondazione IRCCS Policlinico San Matteo and Department of Molecular Medicine, University of Pavia, Italy

[5] Current affiliation: Institute of Neuropathology, Uniklinik RWTH Aachen, Aachen, Germany

[6] Current affiliation: Médecin praticien hospitalier en Neuropathologie chez Hospices Civils de Lyon, France

* These authors contributed equally to this study and should be considered first authors to all effects, regardless of the positioning in the authors' list.

✉ corresponding author: adriano.aguzzi@usz.ch

Abstract

In prion diseases, aggregates of misfolded prion protein (PrP^{Sc}) accumulate not only in the brain but can also be found in various extraneural tissues. This raises the question whether prion-specific pathologies arise also in these tissues. Here we sequenced mRNA transcripts in skeletal muscle, spleen and blood of prion-inoculated mice at eight timepoints during disease progression. We detected consistent gene-expression changes in all three organs, with skeletal muscle showing the most uniform alterations during disease progression. The glutamate synthetase (GLUL) gene was monotonically upregulated in skeletal muscle of mice infected with three different scrapie prion strains (RML, ME7 and 22L) and in human sporadic Creutzfeldt-Jakob disease. GLUL dysregulation was accompanied by changes in glutamate/glutamine metabolism, leading to reduced glutamate levels in skeletal muscle. None of these changes were observed in skeletal muscle of humans with amyotrophic lateral sclerosis, Alzheimer's disease, or dementia with Lewy bodies, suggesting that they are specific to prion diseases. Besides pointing to unrecognized metabolic implications of prion infections, these findings suggest that GLUL could represent an accessible biomarker of prion disease progression, particularly during the preclinical stages of disease, and might be useful for monitoring the efficacy of experimental antiprion therapies.

Introduction

Prions are protein aggregates that cause neurodegenerative diseases of the central nervous system (CNS). Prions multiplicate through the seeded conversion of the physiological cellular prion protein PrP^{C} into a pathologically folded conformer, PrP^{Sc} (Aguzzi and Falsig, 2012). PrP^{C} is expressed not only in the nervous system but also in the skeletal muscle and, to a lesser extent, in lymphoreticular tissue and blood (Tabula Muris et al., 2018; Wulf et al., 2017). Prions can be present in the blood, where they bind to plasminogen (Fischer et al., 2000). Blood is a documented route of infection and remains a challenge for transfusion medicine (Houston et al., 2000; Salamat et al., 2021). Prions can enter the body through the gastrointestinal system and accumulate in lymphoid tissue, leading to neuroinvasion via peripheral nerves (Klein et al., 1997; Mabbott et al., 2000). In variant CJD (vCJD), PrP^{Sc} is present in additional extraneural organs, including the spleen, skeletal muscle, retina, blood vessels, skin, liver, kidney, and pancreas (Notari et al., 2010). Skeletal muscles of both acquired and sporadic CJD patients show PrP^{Sc} deposits mainly localized on nerve fibers (Peden et al., 2006).

The definitive diagnosis of prion diseases relies on the postmortem detection of PrP^{Sc} (Hermann et al., 2021; Llorens et al., 2020). Clinical trials of investigational new drugs require easily accessible and highly specific biomarkers, yet prion replication in brain cannot be assessed non-invasively. Cyclical prion seed amplification can sensitively detect PrP^{Sc} in cerebrospinal fluid (CSF) (Altuna Azkargorta et al., 2022; Hermann et al., 2021) and nasal swab samples (Behaeghe et al., 2018; Di Fede et al., 2018), but variations in sample preparation, equipment, and interpretation criteria can lead to inconsistent results and reduce its reproducibility (Bongianni et al., 2017; Orrú et al., 2017). Moreover, these techniques can generate false-positive results due to the detection of other amyloidogenic proteins, such as Aβ, α-synuclein, and tau (Cramm et al., 2016) and their sensitivity may be influenced by the strain of prions, the stage of disease and the tissue source used for the assay (Cramm et al., 2016; Hermann et al., 2021). Other often used biomarkers, such as 14-3-3 and total tau protein in CSF, lack specificity to PrDs (Stoeck et al., 2012). Emerging biomarkers, such as neurofilament light polypeptide and YKL-40, show promise as combinatorial approaches to rule out the diagnosis of prion diseases (Mok and Mead, 2020; Zerr et al., 2018), and peripheral blood derived from sCJD patients has demonstrated considerable potential, with increased levels of neurofilament light polypeptide reliably reflecting the levels in CSF (Abu-Rumeileh et al., 2020).

Several studies have shown that gene expression changes in skeletal muscle can be used to monitor the progression of neurodegenerative diseases. Muscle-specific genes are downregulated in patients with Huntington's disease, suggesting their potential use for

monitoring disease progression (Strand et al., 2005). Similarly, (Henley et al., 2005) found that the expression of genes related to muscle function was decreased in patients with Alzheimer's disease. In another study, (Pradat et al., 2011) identified a set of muscle-specific genes that were differentially expressed in patients with amyotrophic lateral sclerosis (ALS). Lymphoid tissue also accumulates prions (Aguzzi et al., 2013; Halliez et al., 2014) and may experience molecular changes with diagnostic and prognostic potential.

Here we have conducted transcriptome-wide RNA sequencing analyses on blood, skeletal muscle, and spleen of mice after intracerebral exposure to prions and in skeletal muscle of humans diagnosed with sporadic CJD. We found that glutamate synthetase (GLUL) is uniquely upregulated in skeletal muscle of prion-infected mice and humans, but not in Amyotrophic Lateral Sclerosis (ALS), Alzheimer's Disease (AD), and Dementia with Lewy Bodies (DLB). Besides pointing to an unappreciated link between prion infection and GLUL dysregulation, the specificity of this finding suggests that analyses of the biosynthetic glutamine pathway may yield early biomarkers of prion diseases.

Results

Transcriptional analyses reveal recurrent derangement in skeletal muscle during prion disease progression.

We injected intracerebrally (i.c.) wild-type 2-month old C57BL/6 mice with scrapie prions (6th consecutive mouse-to-mouse passage of mouse-adapted Rocky Mountain Laboratory sheep scrapie prions, abbreviated as RML6). For control, we injected non-infectious brain homogenate (NBH). Spleen, hindlimb skeletal muscle and blood were collected during necropsy at 4, 8, 12, 14, 16, 18 and 20 weeks-post-inoculation (wpi) as well as at the terminal stage of disease (*Fig. 1a*). We stratified our collective into three categories: early stage (4 and 8 wpi), pre-symptomatic stage (12, 14, 16 wpi) and symptomatic stage (18, 20, wpi and terminal) (Kaczmarczyk et al., 2022) (*Fig. 1a*).

The dimensionality of gene expression patterns across diverse experimental conditions was reduced by Principal Component Analysis (PCA; *Suppl. Fig. 1*). Then, we defined differentially expressed genes (DEGs) as transcripts with absolute $\log_2$ fold change $|\log_2 FC| > 0.5$ and p value < 0.05 (*Fig. 1b)*. Transcriptional changes in blood were inhomogeneous during disease progression (*Fig. 1b – uppermost plot*), possibly because peripheral blood may be subjected to changes in cellular composition during infection or inflammation. Nevertheless, a striking alignment of DEGs associated with blood coagulation and hemostasis was detected across early timepoints (*Suppl. Table 1 and 2*; *Fig. 1c*). During the pre-symptomatic and symptomatic stages, we did not identify any overlapping changes in blood.

In contrast, major transcriptional changes in the spleen were restricted to the terminal stage (*Fig. 1b, middle plot*). Except for *Pcdh18*, which was significantly altered in both early stage timepoints, there was no overlap between DEGs (*Suppl. Table 3*). Compared to other analyzed organs, the number of DEGs in skeletal muscle remained relatively constant throughout the course of the disease (*Fig. 1b, lowermost plot*). However, this consistent pattern was punctuated by the recurrent up or downregulation of specific genes within timepoints corresponding to distinct disease stages; specifically, during the presymptomatic stage, a single gene, *Adh1*, displayed upregulation, whereas the symptomatic stage featured elevated expression of *Mir8114*, *Glul*, and *Pik3r1*. (*Suppl. Table 3*). To allow for interactive exploration of the results described in this study and for integration with our previously reported findings (Sorce et al., 2020), we constructed a searchable database of gene expression profiles

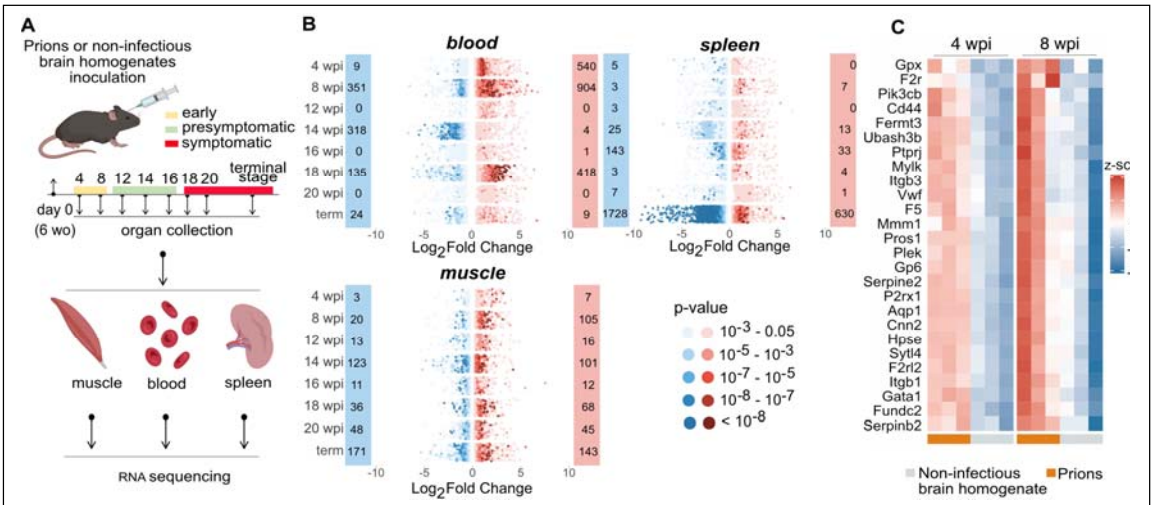

Figure 1. (A) Muscle, blood, and spleen tissues were collected for bulk RNA sequencing at eight individual timepoints (wo = weeks old; wpi = week post inoculation). Samples were stratified into early, presymptomatic, and symptomatic stages. **(B-D) (B)** Prevalence of upregulated (red) and downregulated (blue) DEGs (p-value < 0.05) across disease progression in the three tissues analysed. The dots in the dot plot represent individual genes and are color-coded according to their corresponding p-values. **(C)** Expression patterns of genes related to haemostasis (see Supplementary Figure 1-2 for more details) in blood at 4 and 8 wpi.

from brain and extraneural organs available for visualization and download at https://fgcz-shiny.uzh.ch/priontranscriptomics/. These investigations have also revealed subtle shifts in alternative splicing pattern during prion disease pathogenesis. However, these alterations were transient and variable across timepoints, precluding the use of alternative-splicing based biomarkers unsuitable for diagnostic purposes.

Skeletal muscle shows consistently altered gene modules throughout prion disease progression.

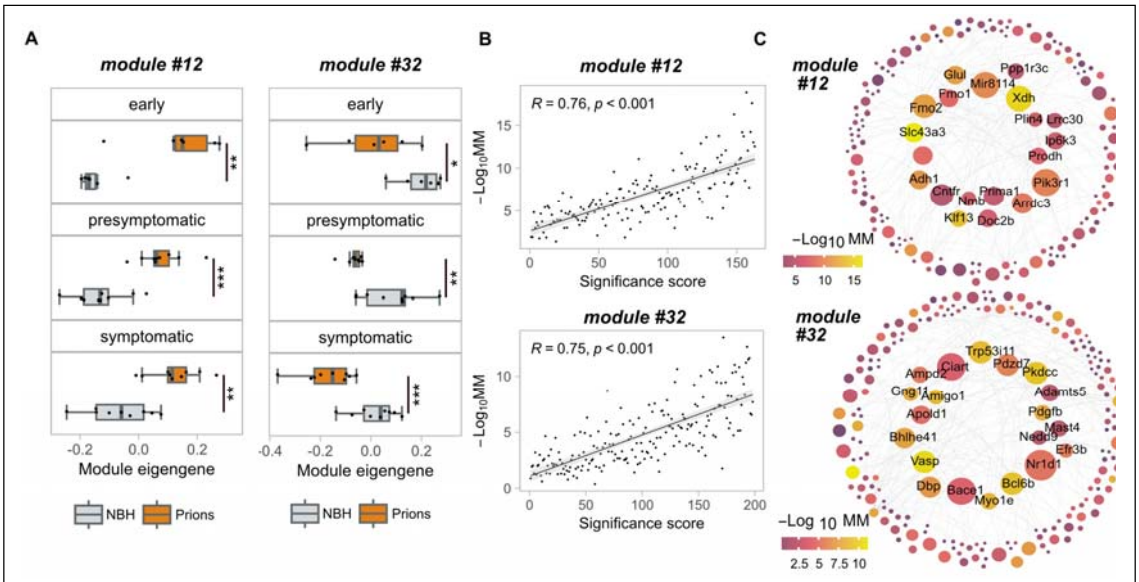

Figure 2 **(A)** Boxplots of module eigengenes of the main cohort for gene co-expression #12 orange and #32 darkgreen modules identified by WGCNA at different timestages (early, presymptomatic and symptomatic). Statistical significance (*p < 0.05, **p < 0.01, ***p < 0.005, ****p < 0.001) is indicated by asterisks **(B)** The scatter plots illustrate the relationship between the significance score (SS) calculated from p-values obtained through differential expression analysis (using DESeq2) and module membership (MM). Pearson correlation coefficient (R) and its corresponding p-value are displayed. **(C)** The minimum spanning trees with nodes representing genes within the #12 orange and #32 darkgreen modules are shown. The colour of each node corresponds to module membership (MM). The size of each node corresponds to its significant score (SS).

WGCNA (Weighted Gene Coexpression Network Analysis) identifies modules of highly correlated genes, enabling the detection of coordinated changes in gene expression. We utilized WGCNA in conjunction with differential expression (DE) analysis to deduce organ-specific gene co-expression networks (*Suppl. Table 4*). To summarize the gene expression levels of individual network modules, we calculated module eigengenes (MEs) representing the first principal component of each module. We identified 25 and 13 modules in blood and spleen, respectively, but we did not find any significant differences between the MEs of these modules in the two study groups across all three disease time stages (*Suppl. Fig*. 2*a,b*). Conversely, in the muscle co-expression network, two of 39 modules (modules #12 and #32) showed significant differences in MEs between non-infectious brain homogenate (NBH) controls and prions throughout disease progression (*Suppl. Fig. 2c*). Module #12 (163 genes) was upregulated, while module #32 (198 genes) was monotonically downregulated as the disease advanced (*Fig. 2a*).

To refine the list of potential biomarkers, we sought to identify the genes with the most prominent and consistent changes throughout disease progression in each module of interest. To this end, we derived a significance score (SS) from p-values obtained through DE analysis with DESeq2. SS was found to be highly correlated (module #12 R = 0.76; and module #32 R = 0.75) with module membership (MM) which is a measure of the correlation

between the expression pattern of a given gene and the overall expression pattern of all the genes within the module (*Fig. 2b*). The convergence of two different methods on the same set of genes provides strong evidence for the robustness of hub gene detection. The top 20 hub genes for #12 and #32 module are labeled in *Fig. 2c*.

Validation cohort confirms robustness of hub genes for muscle co-expression network in prion-infected mice.

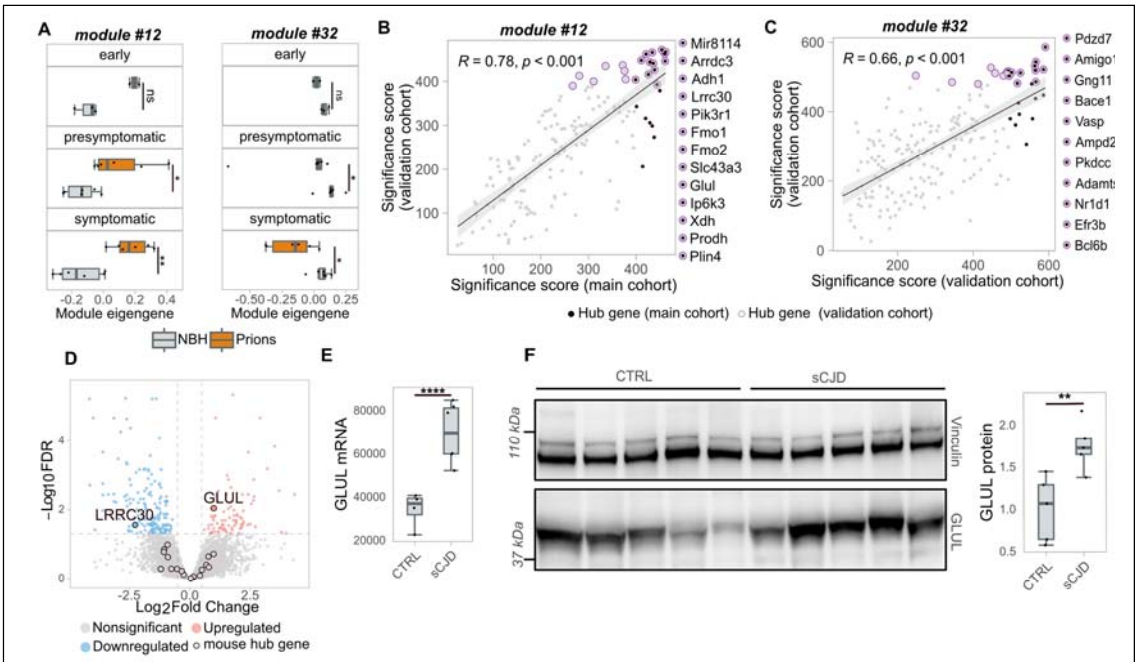

Figure 3 **(A)** Boxplots of module eigengenes of the validation cohort for gene co-expression #12 orange and #32 darkgreen modules identified by WGCNA at different timestages (early, presymptomatic and symptomatic). **(B-C)** The scatter plots (Pearson's correlation and pvalue indicated with R and p, respectively) depict the relationship between genes from the #12 orange and #32 darkgreen modules in the main and validation cohorts. Hub genes detected in the main cohort are represented by black dots, while hub genes detected in the validation cohort are represented by purple-circled dots. The black, purple-circled dots indicate hub genes detected in both cohorts. **(D)** The volcano plot displays the results of bulk RNA sequencing analysis of skeletal muscles from patients with sCJD and their age-matched controls. Red dots represent genes that are significantly upregulated in sCJD, while blue dots represent genes that are significantly downregulated. Mouse hub genes detected in the #12 orange and #32 darkgreen modules are black-circled, indicating their overlap with the DEGs in human samples. **(E)** Normalized counts (Transcript per million, TPM) boxplots of GLUL transcriptional levels in skeletal muscles of sCJD cases and their age-matched controls. **(F)** Western blot analysis (arbitrary densitometry unit, ADU) of GLUL and Vinculin protein expression in skeletal muscle samples from sCJD cases and age-matched controls. Densitometry data is

To ensure the reliability and validity of our findings, we investigated a validation cohort comprising samples from each time stage (*Suppl. Fig. 3a).* We first tested whether the muscle co-expression network modules generated in the main cohort were preserved in the validation cohort. All modules (except for modules #9, #11, and #37) showed high preservation with a z-summary statistic greater than 1.96 (*Suppl. Fig. 3c*). We then calculated the ME for each sample in the validation cohort by using the same gene module assignment as in the main cohort. Once again, the #12 and #32 modules were the most affected, exhibiting significant ME differences between RML6 and NBH at both presymptomatic and symptomatic stages (*Suppl. Fig. 3b*). Notably, the trend of ME changes was already evident in the early stage and consistent with the trend observed in the main cohort (*Fig. 3a*).

To further validate our results, we identified hub genes for the validation cohort using SS values that correlated with those of the main cohort (#12 module R = 0.78; #32 module R =

0.66). The overlapping hub genes between the two cohorts are shown in *Fig. 3b-c*. The high correlation suggests that the hub genes identified in the main cohort were robust and reliable in the validation cohort as well. These findings support the notion that the hub genes identified here are biologically meaningful and may serve as potential biomarkers for the disease.

Prion disease triggers upregulation of glutamine synthase in both human and mouse skeletal muscles

To test whether our findings can be generalized to human prion diseases, we performed RNA sequencing on skeletal muscles of sCJD patients (n = 6) and controls (n = 4) without clinical or pathological diagnosis of neurodegeneration matched for age, gender and specimen age (see *Suppl. Table* 6 for clinical details*).* Although the total RNA extracted from the Psoas major muscle exhibited significant degradation (*Suppl. Fig. 4a*), the removal of ribosomal RNAs unveiled a strong correlation in gene expression within each group. Notably, principal component analysis demonstrated distinct clustering of sCJD and control tissues, indicating a clear separation between the two (*Suppl. Fig. 4b,c*). Based on $|\log_2 FC| > 0.5$ and FDR < 0.05 (see Methods for details), we identified a total of 365 DEGs of which 258 were protein-coding (*Suppl. Table 7*). We compared the DEGs from sCJD samples with hub genes from the two mouse cohorts and found only two overlapping genes. *GLUL* (glutamine synthase) was the only gene significantly upregulated in both human and mouse samples, while *LRRC30* (Leucine Rich Repeat Containing 30), a hub gene in the upregulated #12 module in mouse, was downregulated in human samples (*Fig. 3d,e*). We further validated the upregulation of GLUL at the protein level using Western Blot (*Fig. 3f*). Although our analysis of post-mortem human sCJD muscle samples revealed a significant number of transcriptional changes that did not mirror those observed in animals, it is possible that these alterations were only evident during the advanced stages of the disease, when non-specific changes tend to occur. However, our analysis of mouse models provides strong evidence that GLUL correlates with the disease process at earlier stages.

GLUL is upregulated in mice infected with a variety of prion strains.

Prion strains exhibit distinct biological properties, such as tissue tropism, incubation time, and neuropathological features (Aguzzi et al., 2007) and may elicit different transcriptional responses. We aimed to determine whether GLUL alterations are a common feature across prion strains by testing whether GLUL is changed in mice infected with other mouse-adapted prion strains to a similar extent as in RML6. To this end, we intracerebrally injected an additional cohort of C57BL/6 mice with ME7, 22L, RML6, and NBH and collected hindlimb

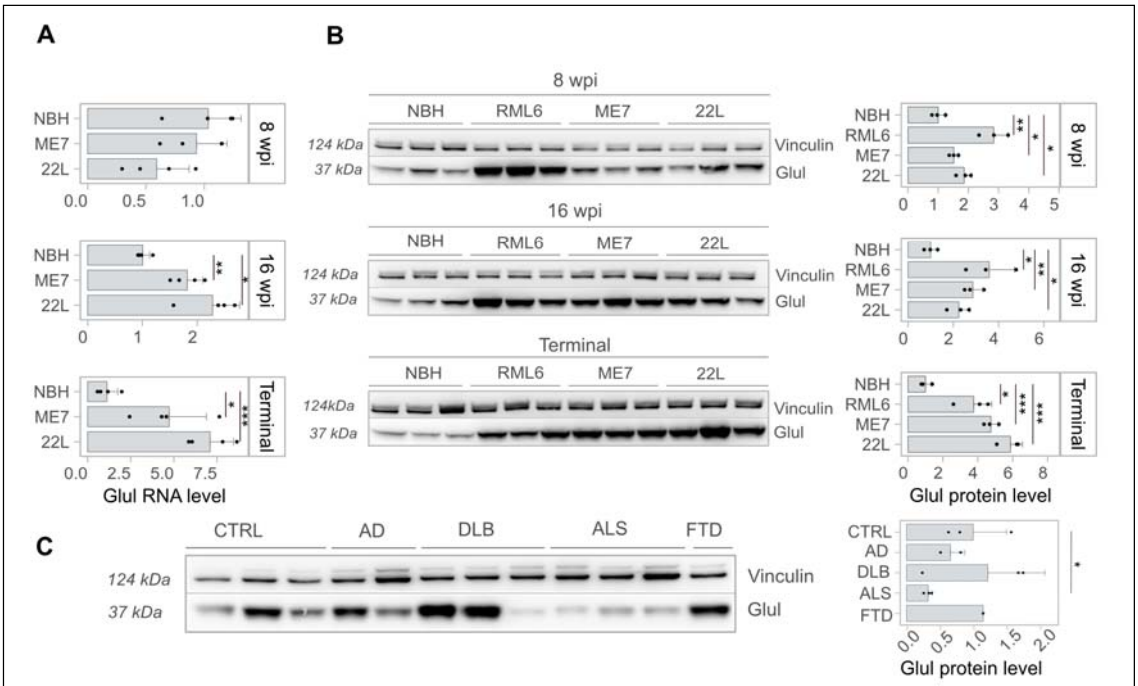

Figure 4. Levels of Glul mRNA, protein, glutamate, and glutamine in skeletal muscle lysates at 8 and 16 weeks post-inoculation (wpi) and terminal stage of mice with prion strains RML6, ME7, and 22L, as well as related control (NBH). In panel **(A)**, barplots display Glul mRNA levels normalized by GAPDH mRNA levels (derived from Ct values via RT-PCR). **(B)** Western blots of Glul and Vinculin protein levels of infected with different prion strains, as well as related NBH control, with densitometry (arbitrary densitometry unit, ADU) data on the right. **(C)** Western blot of Glul and Vinculin protein levels of skeletal muscles from AD, DLB, ALS and FTD diagnosed individuals; related densitometry (ADU) is on the right. Statistical significance (*p < 0.05, **p < 0.01, ***p < 0.005, ****p < 0.001) is indicated by asterisks.

skeletal muscle at different time points (8 wpi, 16 wpi and terminal) corresponding to each of the three defined disease stages. At 8 wpi, *GLUL* RNA levels exhibited stability in both ME7 and 22L strains, yet ME7 and 22L exhibited protein-level upregulation, possibly indicative of RNA degradation during extended sample storage. Notably, the most substantial upregulation at the protein level manifested prominently in RML6-infected animals (*Fig. 4b*). The delayed GLUL upregulation in mice inoculated with the other prion strains could be attributed to differences in disease onset, as RML6-infected animals exhibited a quicker disease onset compared to ME7 and 22L. GLUL expression was significantly altered at both the RNA (*Suppl. Table 7*) and protein level in all strains at 16 wpi and the terminal stage (*Fig. 4a,b*). These results suggest that GLUL upregulation may be a widespread phenomenon across different types of prion diseases, suggesting that it may serve as a general tool for the detection and monitoring of human prion diseases.

GLUL upregulation is specific to prion diseases.

To further investigate the disease specificity of GLUL dysregulation, we examined its protein levels in hindlimb skeletal muscles of mouse models for ALS, AD, and DLB. Unlike prion

diseases, GLUL was not upregulated in these models, making it a promising candidate for distinguishing prion diseases from other neurodegenerative disorders (*Suppl. Fig. 5b*). To corroborate these findings, we extended our investigation to skeletal muscle necropsies from patients with familial ALS, FTD (Frontotemporal Dementia), pure AD, and DLB. Again, we observed that the GLUL protein levels remained statistically unaltered in AD, DLB and FTD, strengthening its candidacy as a specific biomarker for prion diseases. Notably, GLUL protein levels were significantly downregulated in all three individuals affected by ALS (*Fig. 4c*).

Glutamate-glutamine biosynthesis in muscle is affected during prion disease progression.

GLUL catalyzes the conversion of glutamate to glutamine. Given the increased expression of GLUL in skeletal muscle during prion disease progression, we investigated whether this metabolic pathway was affected. We measured glutaminase, glutamate and glutamine levels in muscle lysates from C57BL/6 mice inoculated with ME7, 22L and RML6 brain homogenates, as well as NBH for control. At the early disease stage, there were no significant alterations in the levels of glutamate and glutamine, even in RML6-infected animals, despite the increased expression levels of GLUL (*Suppl. Fig. 5c*). This might be attributable to a potential compensatory effect of glutaminase upregulation (*Suppl. Fig. 5a*), which may maintain glutamate homeostasis and, in turn, offset the increased expression of GLUL. Notably, we observed an increase in the expression of GLUL at 16 wpi (two weeks prior to the onset of clinical signs of prion disease). Despite the upregulation of GLUL, the balance of glutamate and glutamine was maintained (*Suppl. Fig. 5c*), as well as glutaminase levels (*Suppl. Fig. 5a*), pointing to a metabolic ability restoring the levels of glutamate consumed by GLUL upregulation. At the terminal stage of the disease, the levels of glutamate were notably reduced (*Suppl. Fig. 5c*), plausibly due to a significant upregulation of GLUL. However, the levels of glutamine and glutaminase were unchanged (*Suppl. Fig. 5a,c*), despite the expectation that they would increase as a compensatory mechanism for the decrease in glutamate. Glutamate reduction was also detected in necropsies of sCJD patients versus age- and sex-matched controls (*Suppl. Fig. 5d)*.

We then examined the levels of glutaminase, glutamate, and glutamine in skeletal muscles of aged animal models for AD, DLB, and ALS. Unlike in prion diseases, we found no significant alterations in glutaminase, glutamate and glutamine levels in these neurodegenerative disorders. This highlights the specificity of the observed metabolic changes in prion diseases and emphasizes the potential of GLUL as a distinctive biomarker. Furthermore, our investigations extended to human cases of AD, DLB, ALS, and FTD, where we evaluated glutamate and glutamine levels in skeletal muscles. Interestingly, our results

revealed a reduction in glutamate levels solely in the context of ALS, mirroring the observed trend in prion diseases (*Suppl. Fig. 5b,e*). However, it is important to note that while GLUL expression is downregulated in ALS, it is upregulated in prion diseases.

Discussion

Transcriptional changes occurring in the early phase of prion disease may help for the early detection and diagnosis of prion diseases (PrDs), while also pointing to pathogenic mechanisms operating in extraneural organs. Here we conducted a comprehensive transcriptomic characterization of extraneural organs known to harbor prions. We hypothesized that the presence of prions in these organs could result in changes to RNA processing, or modifications to the abundance of specific transcripts. By examining multiple timepoints throughout the progression of the disease in prion-inoculated mice, we focused on identifying recurrent changes that could aid in the detection of PrDs before the onset of clinical symptoms.

Significant changes in gene expression were observed in all three organs. In the spleen, major transcriptional alterations were detected only at the terminal stage of the disease, which suggests a slower accumulation rate of prions in lymphatic tissue following intracerebral inoculation compared to ingestion or intraperitoneal inoculation. On the other hand, blood samples displayed upregulation of numerous transcripts during the early stages of prion exposure, of which a significant fraction was related to hemostasis.

Gene-expression changes were detected in both blood and spleen, but were not consistent across all timepoints. However, the transcriptome of skeletal muscle showed consistent alterations throughout the disease progression. Using WGCNA, we identified two primary gene subsets in skeletal muscle exhibiting progressive changes that became evident in the early stage of disease. Validation of these findings in an independent cohort of mice, in which sequencing libraries were prepared several months after RNA extraction from snap-frozen skeletal muscles by a different researcher, enhances the robustness of the results. This validation underscores the consistency of the findings, even in the face of significant technical variability introduced by the procedures. These results have potential applications in monitoring disease progression following therapeutics administration, in conjunction with molecular and behavioral assessments for evaluating treatment efficacy (Bender et al., 2019; Bradley et al., 2017; Skinner et al., 2015).

We evaluated the relevance of our findings in humans by conducting bulk RNA sequencing on skeletal muscle samples obtained from individuals with sCJD and control individuals without neurological impairments. While we were unable to confidently evaluate the level of preservation of mouse and human muscle gene-expression networks, we found little overlap

between the joint set of hub genes identified across two mouse cohorts and human DEGs. There may be various reasons for this discrepancy, including the genetic differences between mice and humans which may result in varying biological responses to the same disease (Perlman, 2016). Additionally, different conditions were employed to process the human samples and decontaminate them from prions, which may have influenced the results (Scholes and Lewis, 2020). Variations in disease stage or severity, as well as differences in the tissue types analyzed (hindlimb muscle in animals vs. psoas muscle in humans), could have also played a role in the observed differences (Terry et al., 2018). Finally, there may be underlying differences in the disease biology between humans and mice that are not yet fully understood or characterized (Swearengen, 2018). Despite the abovementioned limitations in translating mouse findings to human ones, we found that *Glul*, which was a strong hub gene in the upregulated #12 module in the mouse study, was significantly upregulated in human sCJD samples, as confirmed at the protein level by Western Blot analysis. Hence, GLUL may have potential to serve as a biomarker to detect and track the progression of prion disease, particularly during the earlier stages. GLUL is a glutamate-ammonia ligase that catalyzes the synthesis of glutamine from glutamate and ammonia in an ATP-dependent reaction.

There is some evidence that GLUL expression in the brain is not altered in PrDs. *GLUL* mRNA levels were unchanged in the brains of mice infected with prions compared to uninfected mice (Sorce et al., 2020). Another recent study found that *GLUL* expression was also unchanged in the brains of patients with sCJD compared to healthy controls (Dimitriadis et al., 2022). Therefore, the alterations in glutamate/glutamine metabolism in prion-infected brains (Bourgognon et al., 2018) that were proposed to contribute to neurodegeneration and cognitive dysfunctions, are unlikely to stem from any changes in brain-resident GLUL. Instead, GLUL expression was consistently upregulated in the skeletal muscles of animals throughout the disease, and this finding was present after infection with multiple prion strains. This suggests that GLUL may also be upregulated before the clinical onset of human PrDs. The identification of a common pathological phenotype among these diseases would be a significant finding, as it could provide a potential diagnostic biomarker specific to these conditions. It is important to note that this phenomenon appears to be unique to these diseases and does not occur in other common neurodegenerative disorders such as ALS, AD, or DLB; interestingly, GLUL protein levels were consistently found to be downregulated in human ALS. suggesting a possible association between reduced GLUL expression and the pathogenesis of ALS. This emphasizes the exceptional applicability of this biomarker to prion diseases. The identification of a specific biomarker for these diseases is critical for

early diagnosis and intervention, which could improve treatment outcomes and patient survival.

We hypothesized that the upregulation of GLUL protein in skeletal muscle may be linked to a metabolic dysfunction in the glutamate-glutamine pathway. Prior research had shown the direct influence of glutamine levels on the expression of GLUL in skeletal muscle cells (Huang et al., 2007). Building upon this finding, it is plausible to speculate that a potential systemic deficit in glutamine levels might contribute to the observed upregulation of GLUL in skeletal muscle. Skeletal muscle exerts a pivotal role in glutamine storage, production, and release into the bloodstream. This hypothesis gains further support from the significant reduction in glutamate levels observed, which could be attributed to the heightened activity of GLUL in response to altered glutamine availability. This was unexpected as previous studies had reported increased levels of glutamate and glutamine in the brain and cerebrospinal fluid of patients with neurodegenerative diseases, including prion diseases (Bourgognon et al., 2018). These findings suggest that the regulation of glutamate and glutamine metabolism in skeletal muscle differs from that in the brain, and that the upregulation of GLUL in skeletal muscle may have a distinct role in the pathology of prion disease. In contrast, the absence of such GLUL upregulation in other NDDs might signify a distinct metabolic response. The lack of compensatory GLUL expression could contribute to the sustained alterations in glutamine and glutamate levels seen in those conditions. Therefore, the specific association between GLUL upregulation and prion diseases may offer a unique mechanistic insight into the intricate interplay between glutamine/glutamate metabolism and disease progression, setting prion diseases apart from other NDDs. Further research into these connections may validate GLUL levels as an easily accessible biomarker which could be useful for monitoring the efficacy of experimental antiprion therapies.

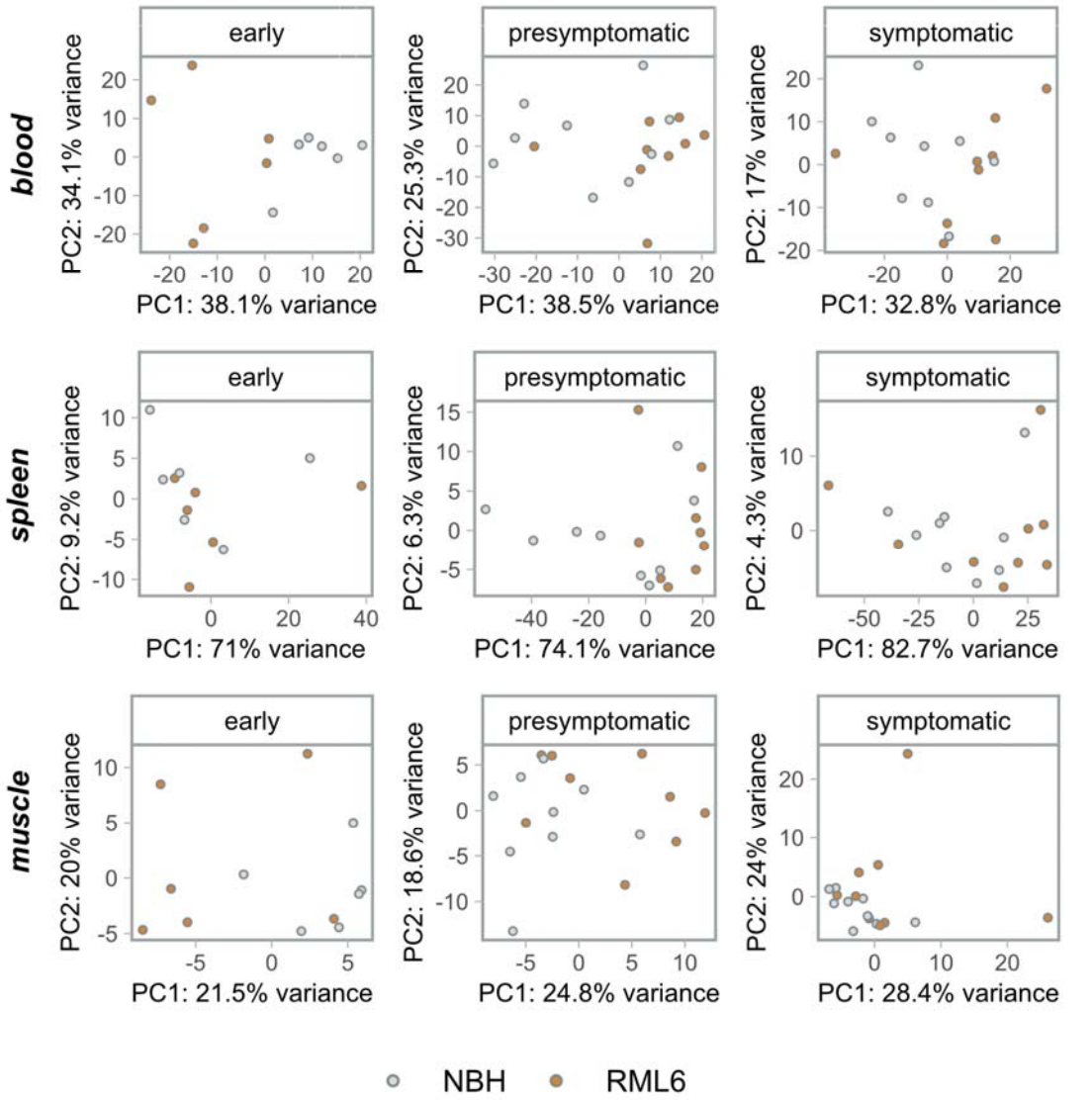

Suppl. Fig. 1. PCA (principal component analysis) of RNA-seq data across three timestages (early, symptomatic, and terminal) and three organs (blood, muscle, and spleen). Each point on the plot represents a sample.

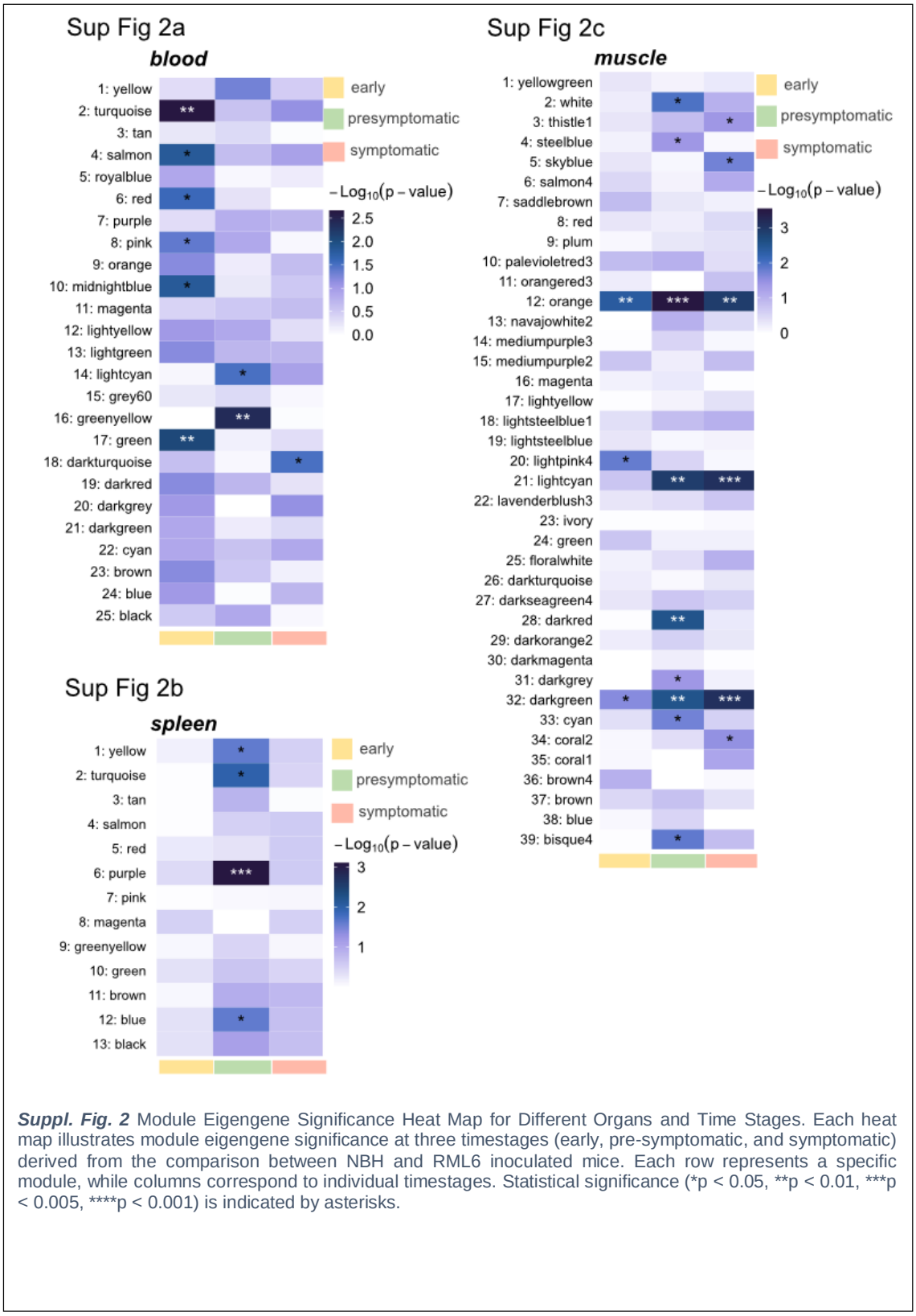

Suppl. Fig. 2 Module Eigengene Significance Heat Map for Different Organs and Time Stages. Each heat map illustrates module eigengene significance at three timestages (early, pre-symptomatic, and symptomatic) derived from the comparison between NBH and RML6 inoculated mice. Each row represents a specific module, while columns correspond to individual timestages. Statistical significance (*p < 0.05, **p < 0.01, ***p < 0.005, ****p < 0.001) is indicated by asterisks.

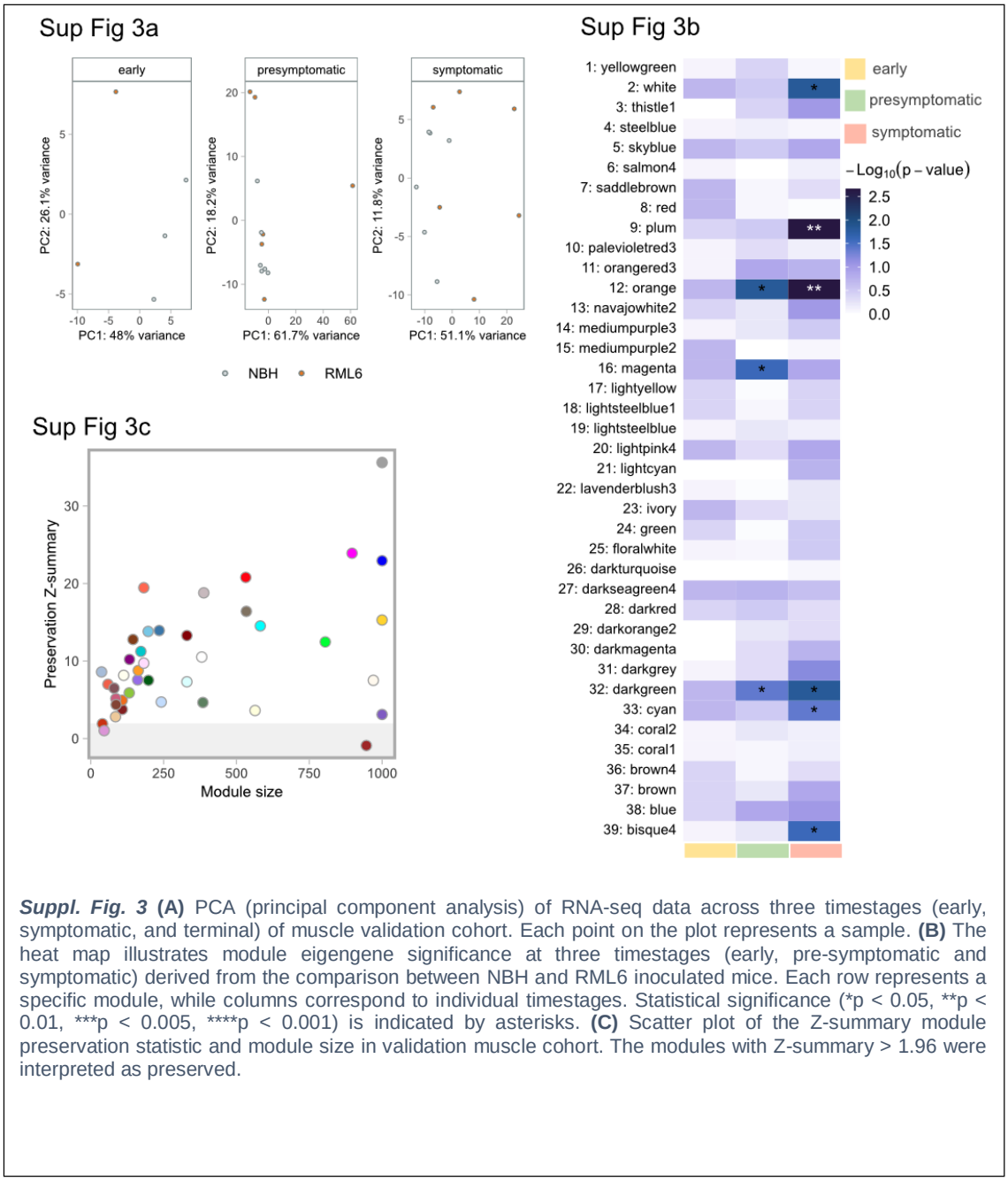

Suppl. Fig. 3 **(A)** PCA (principal component analysis) of RNA-seq data across three timestages (early, symptomatic, and terminal) of muscle validation cohort. Each point on the plot represents a sample. **(B)** The heat map illustrates module eigengene significance at three timestages (early, pre-symptomatic and symptomatic) derived from the comparison between NBH and RML6 inoculated mice. Each row represents a specific module, while columns correspond to individual timestages. Statistical significance (*p < 0.05, **p < 0.01, ***p < 0.005, ****p < 0.001) is indicated by asterisks. **(C)** Scatter plot of the Z-summary module preservation statistic and module size in validation muscle cohort. The modules with Z-summary > 1.96 were interpreted as preserved.

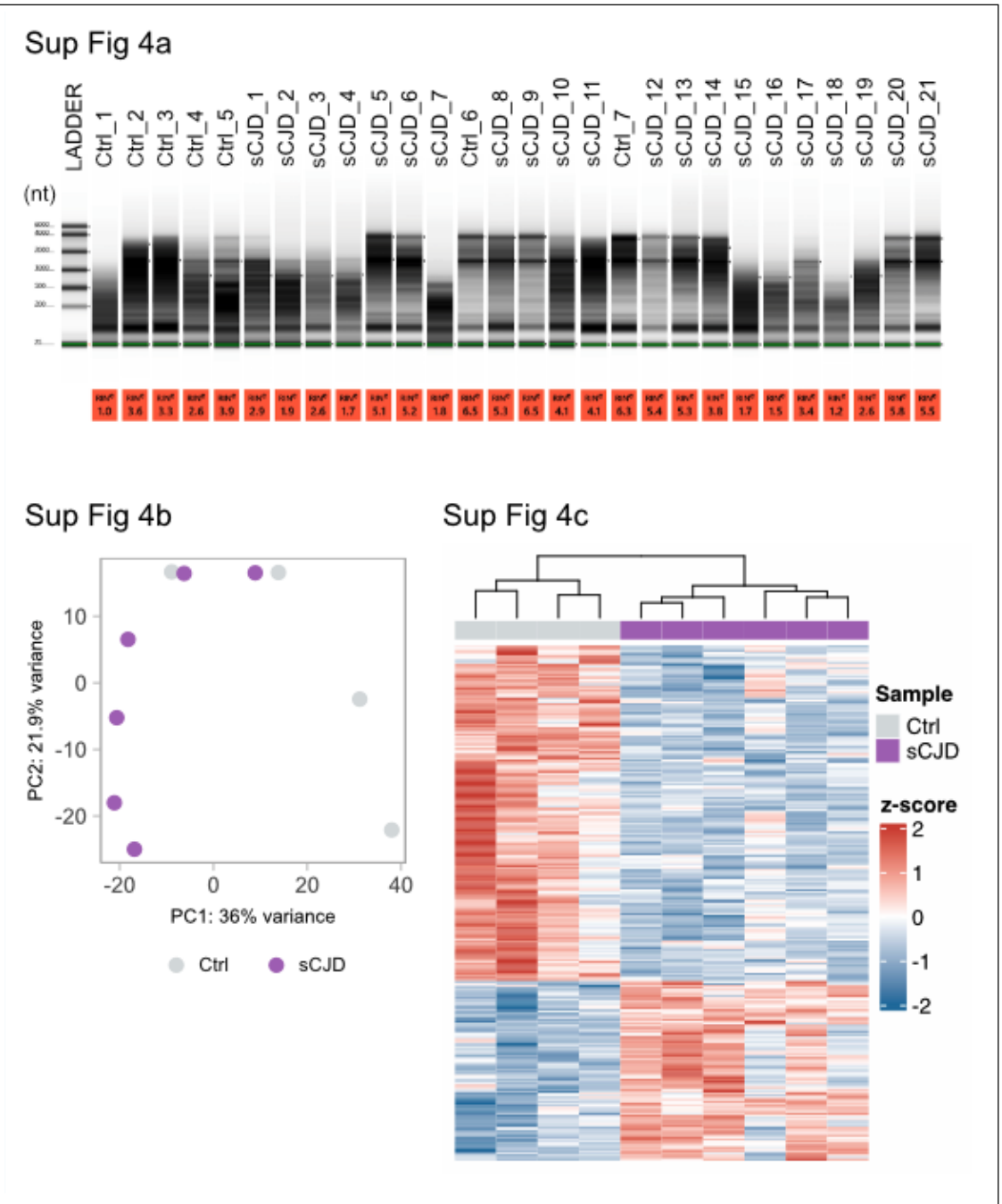

Suppl. Fig. 4 **(A)** Agilent Bioanalyzer gel image depicting total RNA samples extracted from skeletal muscle tissues of both sCJD patients and control subjects**.** The image showcases the RNA quality assessment using the Ribosomal Integrity Number (RIN) scores, displayed alongside the respective samples. **(B)** Principal Component Analysis (PCA) plot illustrating the segregation of gene expression profiles in skeletal muscle samples between individuals with sCJD and non-sCJD controls. Each data point represents a distinct sample, with color coding indicating the differentiation between the two sample conditions**. (C)** Heat Map illustrating the variation in gene expression between individuals with sCJD and non-sCJD controls. Each row corresponds to a differentially expressed gene, while each column represents an individual subject from either the sCJD or control group. Z-scores are color-coded, with red denoting upregulated gene expression and blue representing downregulated expression.

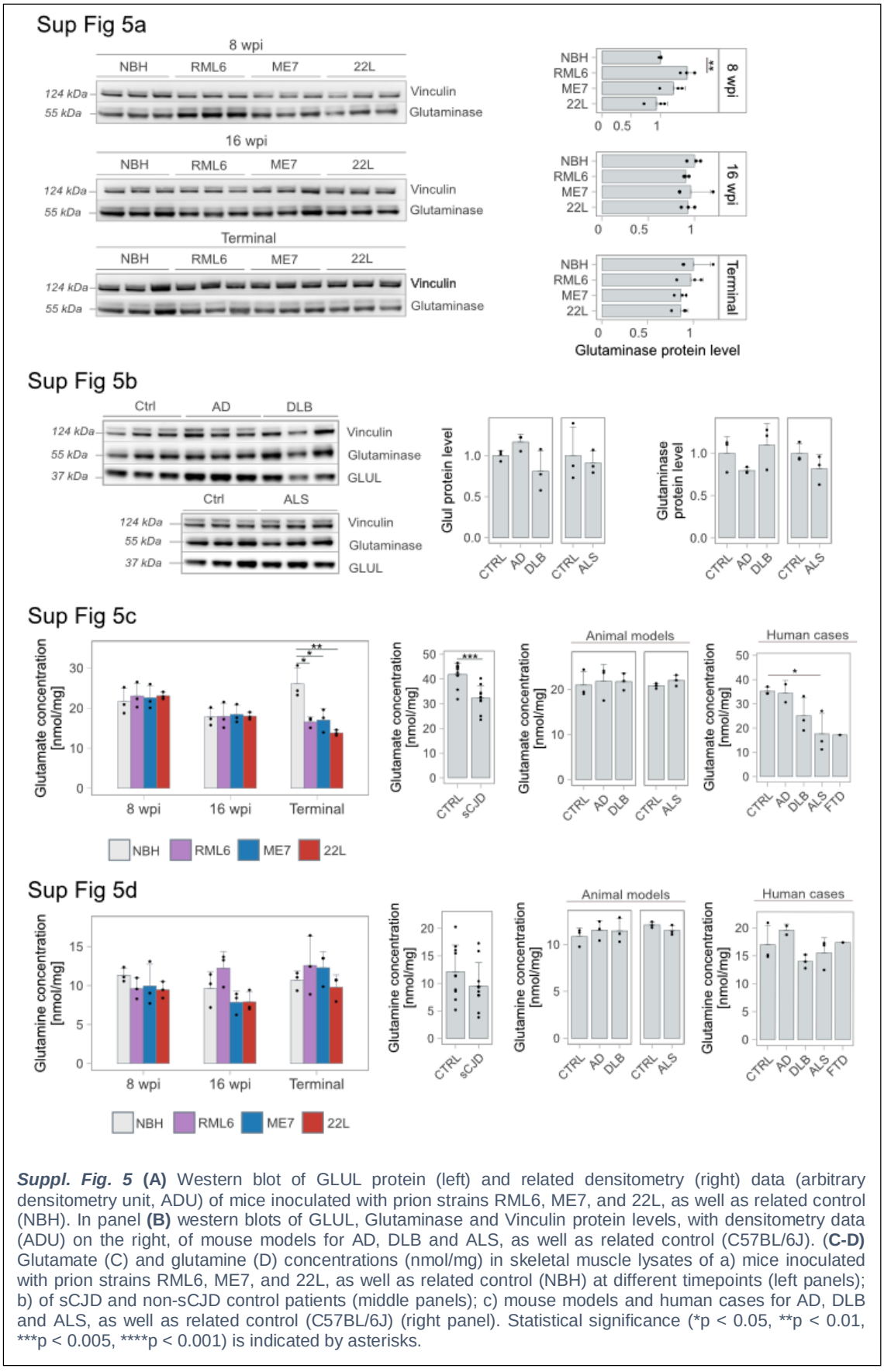

Suppl. Fig. 5 **(A)** Western blot of GLUL protein (left) and related densitometry (right) data (arbitrary densitometry unit, ADU) of mice inoculated with prion strains RML6, ME7, and 22L, as well as related control (NBH). In panel **(B)** western blots of GLUL, Glutaminase and Vinculin protein levels, with densitometry data (ADU) on the right, of mouse models for AD, DLB and ALS, as well as related control (C57BL/6J). (**C-D)** Glutamate (C) and glutamine (D) concentrations (nmol/mg) in skeletal muscle lysates of a) mice inoculated with prion strains RML6, ME7, and 22L, as well as related control (NBH) at different timepoints (left panels); b) of sCJD and non-sCJD control patients (middle panels); c) mouse models and human cases for AD, DLB and ALS, as well as related control (C57BL/6J) (right panel). Statistical significance (*p < 0.05, **p < 0.01, ***p < 0.005, ****p < 0.001) is indicated by asterisks.

References

Abu-Rumeileh, S., S. Baiardi, A. Ladogana, C. Zenesini, A. Bartoletti-Stella, A. Poleggi, A. Mammana, B. Polischi, M. Pocchiari, S. Capellari, and P. Parchi. 2020. Comparison between plasma and cerebrospinal fluid biomarkers for the early diagnosis and association with survival in prion disease. *Journal of Neurology, Neurosurgery & Psychiatry*. 91:1181-1188.

Aguzzi, A., and J. Falsig. 2012. Prion propagation, toxicity and degradation. *Nat Neurosci*. 15:936-939.

Aguzzi, A., M. Heikenwalder, and M. Polymenidou. 2007. Insights into prion strains and neurotoxicity. *Nature Reviews Molecular Cell Biology*. 8:552-561.

Aguzzi, A., M. Nuvolone, and C. Zhu. 2013. The immunobiology of prion diseases. *Nature reviews. Immunology*. 13:888-902.

Altuna Azkargorta, M., Í. Ruiz, M.V. Zelaya Huerta, and M. Mendióroz Iriarte. 2022. Role of biomarkers for the diagnosis of prion diseases: a narrative review. *Medicina-lithuania, 2022, 58 (4), 473*.

Anders, S., A. Reyes, and W. Huber. 2012. Detecting differential usage of exons from RNA-seq data. *Genome Res*. 22:2008-2017.

Behaeghe, O., E. Mangelschots, B. De Vil, and P. Cras. 2018. A systematic review comparing the diagnostic value of 14-3-3 protein in the cerebrospinal fluid, RT-QuIC and RT-QuIC on nasal brushing in sporadic Creutzfeldt–Jakob disease. *Acta Neurologica Belgica*. 118:395-403.

Bender, H., N. Noyes, J.L. Annis, A. Hitpas, L. Mollnow, K. Croak, S. Kane, K. Wagner, S. Dow, and M. Zabel. 2019. PrPC knockdown by liposome-siRNA-peptide complexes (LSPCs) prolongs survival and normal behavior of prion-infected mice immunotolerant to treatment. *PloS one*. 14:e0219995.

Bongianni, M., C. Orrù, B.R. Groveman, L. Sacchetto, M. Fiorini, G. Tonoli, G. Triva, S. Capaldi, S. Testi, S. Ferrari, A. Cagnin, A. Ladogana, A. Poleggi, E. Colaizzo, D. Tiple, L. Vaianella, S. Castriciano, D. Marchioni, A.G. Hughson, D. Imperiale, T. Cattaruzza, G.M. Fabrizi, M. Pocchiari, S. Monaco, B. Caughey, and G. Zanusso. 2017. Diagnosis of Human Prion Disease Using Real-Time Quaking-Induced Conversion Testing of Olfactory Mucosa and Cerebrospinal Fluid Samples. *JAMA Neurology*. 74:155-162.

Bourgognon, J.-M., J.G. Spiers, H. Scheiblich, A. Antonov, S.J. Bradley, A.B. Tobin, and J.R. Steinert. 2018. Alterations in neuronal metabolism contribute to the pathogenesis of prion disease. *Cell Death & Differentiation*. 25:1408-1425.

Bradley, S.J., J.-M. Bourgognon, H.E. Sanger, N. Verity, A.J. Mogg, D.J. White, A.J. Butcher, J.A. Moreno, C. Molloy, T. Macedo-Hatch, J.M. Edwards, J. Wess, R. Pawlak, D.J. Read, P.M. Sexton, L.M. Broad, J.R. Steinert, G.R. Mallucci, A. Christopoulos, C.C. Felder, and A.B. Tobin. 2017. M1 muscarinic allosteric modulators slow prion neurodegeneration and restore memory loss. *The Journal of Clinical Investigation*. 127:487-499.

Cramm, M., M. Schmitz, A. Karch, E. Mitrova, F. Kuhn, B. Schroeder, A. Raeber, D. Varges, Y.-S. Kim, K. Satoh, S. Collins, and I. Zerr. 2016. Stability and Reproducibility Underscore Utility of RT-QuIC for Diagnosis of Creutzfeldt-Jakob Disease. *Molecular Neurobiology*. 53:1896-1904.

Di Fede, G., G. Giaccone, M. Salmona, and F. Tagliavini. 2018. Translational research in Alzheimer's and Prion diseases. *Journal of Alzheimer's Disease*. 62:1247-1259.

Dimitriadis, A., F. Zhang, T. Murphy, T. Trainer, Z. Jaunmuktane, C. Schmidt, T. Nazari, J. Linehan, S. Brandner, J. Collinge, S. Mead, and E. Viré. 2022. Single-nuclei transcriptomics of mammalian prion diseases identifies dynamic gene signatures shared between species. *bioRxiv*:2022.2009.2013.507650.

Dobin, A., C.A. Davis, F. Schlesinger, J. Drenkow, C. Zaleski, S. Jha, P. Batut, M. Chaisson, and T.R. Gingeras. 2013. STAR: ultrafast universal RNA-seq aligner. *Bioinformatics*. 29:15-21.

Dobrowolny, G., M. Martini, B.M. Scicchitano, V. Romanello, S. Boncompagni, C. Nicoletti, L. Pietrangelo, S. De Panfilis, A. Catizone, M. Bouchè, M. Sandri, R. Rudolf, F. Protasi, and A.

Musarò. 2017. Muscle Expression of SOD1G93A Triggers the Dismantlement of Neuromuscular Junction via PKC-Theta. *Antioxidants & Redox Signaling*. 28:1105-1119.

Fischer, M.B., C. Roeckl, P. Parizek, H.P. Schwarz, and A. Aguzzi. 2000. Binding of disease-associated prion protein to plasminogen. *Nature*. 408:479-483.

Goldstein, L.D., Y. Cao, G. Pau, M. Lawrence, T.D. Wu, S. Seshagiri, and R. Gentleman. 2016. Prediction and Quantification of Splice Events from RNA-Seq Data. *PloS one*. 11:e0156132.

Halliez, S., F. Reine, L. Herzog, E. Jaumain, S. Haïk, H. Rezaei, J.-L. Vilotte, H. Laude, and V. Béringue. 2014. Accelerated, Spleen-Based Titration of Variant Creutzfeldt-Jakob Disease Infectivity in Transgenic Mice Expressing Human Prion Protein with Sensitivity Comparable to That of Survival Time Bioassay. *Journal of virology*. 88:8678-8686.

Hatakeyama, M., L. Opitz, G. Russo, W.H. Qi, R. Schlapbach, and H. Rehrauer. 2016. SUSHI: an exquisite recipe for fully documented, reproducible and reusable NGS data analysis. *Bmc Bioinformatics*. 17.

Henley, S.M., G.P. Bates, and S.J. Tabrizi. 2005. Biomarkers for neurodegenerative diseases. *Current Opinion in Neurology*. 18:698-705.

Hermann, P., B. Appleby, J.-P. Brandel, B. Caughey, S. Collins, M.D. Geschwind, A. Green, S. Haïk, G.G. Kovacs, A. Ladogana, F. Llorens, S. Mead, N. Nishida, S. Pal, P. Parchi, M. Pocchiari, K. Satoh, G. Zanusso, and I. Zerr. 2021. Biomarkers and diagnostic guidelines for sporadic Creutzfeldt-Jakob disease. *The Lancet Neurology*. 20:235-246.

Hill, A.F., S. Joiner, J.D.F. Wadsworth, K.C.L. Sidle, J.E. Bell, H. Budka, J.W. Ironside, and J. Collinge. 2003. Molecular classification of sporadic Creutzfeldt-Jakob disease. *Brain : a journal of neurology*. 126:1333-1346.

Houston, F., J.D. Foster, A. Chong, N. Hunter, and C.J. Bostock. 2000. Transmission of BSE by blood transfusion in sheep. *Lancet*. 356:999-1000.

Huang, Y.-F., Y. Wang, and M. Watford. 2007. Glutamine Directly Downregulates Glutamine Synthetase Protein Levels in Mouse C2C12 Skeletal Muscle Myotubes12. *The Journal of Nutrition*. 137:1357-1362.

Kaczmarczyk, L., M. Schleif, L. Dittrich, R.H. Williams, M. Koderman, V. Bansal, A. Rajput, T. Schulte, M. Jonson, C. Krost, F.J. Testaquadra, S. Bonn, and W.S. Jackson. 2022. Distinct translatome changes in specific neural populations precede electroencephalographic changes in prion-infected mice. *PLOS Pathogens*. 18:e1010747.

Klein, M.A., R. Frigg, E. Flechsig, A.J. Raeber, U. Kalinke, H. Bluethmann, F. Bootz, M. Suter, R.M. Zinkernagel, and A. Aguzzi. 1997. A crucial role for B cells in neuroinvasive scrapie. *Nature*. 390:687-690.

Langfelder, P., and S. Horvath. 2008. WGCNA: an R package for weighted correlation network analysis. *BMC Bioinformatics*. 9:559.

Llorens, F., N. Rübsamen, P. Hermann, M. Schmitz, A. Villar-Piqué, S. Goebel, A. Karch, and I. Zerr. 2020. A prognostic model for overall survival in sporadic Creutzfeldt-Jakob disease. *Alzheimer's & Dementia*. 16:1438-1447.

Love, M.I., W. Huber, and S. Anders. 2014. Moderated estimation of fold change and dispersion for RNA-seq data with DESeq2. *Genome biology*. 15:550.

Mabbott, N.A., F. Mackay, F. Minns, and M.E. Bruce. 2000. Temporary inactivation of follicular dendritic cells delays neuroinvasion of scrapie. *Nature medicine*. 6:719-720.

Mok, T.H., and S. Mead. 2020. Preclinical biomarkers of prion infection and neurodegeneration. *Current Opinion in Neurobiology*. 61:82-88.

Notari, S., F.J. Moleres, S.B. Hunter, E.D. Belay, L.B. Schonberger, I. Cali, P. Parchi, W.J. Shieh, P. Brown, S. Zaki, W.Q. Zou, and P. Gambetti. 2010. Multiorgan Detection and Characterization of Protease-Resistant Prion Protein in a Case of Variant CJD Examined in the United States. *PloS one*. 5.

Orrú, C.D., J. Yuan, B.S. Appleby, B. Li, Y. Li, D. Winner, Z. Wang, Y.-A. Zhan, M. Rodgers, J. Rarick, R.E. Wyza, T. Joshi, G.-X. Wang, M.L. Cohen, S. Zhang, B.R. Groveman, R.B. Petersen, J.W.

Ironside, M.E. Quiñones-Mateu, J.G. Safar, Q. Kong, B. Caughey, and W.-Q. Zou. 2017. Prion seeding activity and infectivity in skin samples from patients with sporadic Creutzfeldt-Jakob disease. *Science translational medicine*. 9:eaam7785.

Peden, A.H., D.L. Ritchie, M.W. Head, and J.W. Ironside. 2006. Detection and localization of PrPSc in the skeletal muscle of patients with variant, latrogenic, and sporadic forms of Creutzfeldt-Jakob disease. *American Journal of Pathology*. 168:927-935.

Perlman, R.L. 2016. Mouse models of human disease: An evolutionary perspective. *Evolution, Medicine, and Public Health*. 2016:170-176.

Pradat, P.-F., O. Dubourg, M. de Tapia, F. di Scala, L. Dupuis, T. Lenglet, G. Bruneteau, F. Salachas, L. Lacomblez, J.-C. Corvol, P. Demougin, M. Primig, V. Meininger, J.-P. Loeffler, and J.-L. Gonzalez de Aguilar. 2011. Muscle Gene Expression Is a Marker of Amyotrophic Lateral Sclerosis Severity. *Neurodegenerative Diseases*. 9:38-52.

Salamat, M.K.F., A.R.A. Blanco, S. McCutcheon, K.B. Tan, P. Stewart, H. Brown, A. Smith, C. de Wolf, M.H. Groschup, and D. Becher. 2021. Preclinical transmission of prions by blood transfusion is influenced by donor genotype and route of infection. *PLoS pathogens*. 17:e1009276.

Scholes, A.N., and J.A. Lewis. 2020. Comparison of RNA isolation methods on RNA-Seq: implications for differential expression and meta-analyses. *BMC Genomics*. 21:249.

Skinner, P.J., H.O. Kim, D. Bryant, N.J. Kinzel, C. Reilly, S.A. Priola, A.E. Ward, P.A. Goodman, K. Olson, and D.M. Seelig. 2015. Treatment of Prion Disease with Heterologous Prion Proteins. *PloS one*. 10:e0131993.

Sorce, S., M. Nuvolone, G. Russo, A. Chincisan, D. Heinzer, M. Avar, M. Pfammatter, P. Schwarz, M. Delic, M. Muller, S. Hornemann, D. Sanoudou, C. Scheckel, and A. Aguzzi. 2020. Genome-wide transcriptomics identifies an early preclinical signature of prion infection. *PLoS Pathog*. 16:e1008653.

Stoeck, K., P. Sanchez-Juan, J. Gawinecka, A. Green, A. Ladogana, M. Pocchiari, R. Sanchez-Valle, E. Mitrova, T. Sklaviadis, J. Kulczycki, D. Slivarichova, A. Saiz, M. Calero, R. Knight, A. Aguzzi, J.L. Laplanche, K. Peoc'h, G. Schelzke, A. Karch, C.M. van Duijn, and I. Zerr. 2012. Cerebrospinal fluid biomarker supported diagnosis of Creutzfeldt-Jakob disease and rapid dementias: a longitudinal multicentre study over 10 years. *Brain : a journal of neurology*. 135:3051-3061.

Strand, A.D., A.K. Aragaki, D. Shaw, T. Bird, J. Holton, C. Turner, S.J. Tapscott, S.J. Tabrizi, A.H. Schapira, C. Kooperberg, and J.M. Olson. 2005. Gene expression in Huntington's disease skeletal muscle: a potential biomarker. *Human molecular genetics*. 14:1863-1876.

Swearengen, J.R. 2018. Choosing the right animal model for infectious disease research. *Animal Models and Experimental Medicine*. 1:100-108.

Tabula Muris, C., c. Overall, c. Logistical, c. Organ, processing, p. Library, sequencing, a. Computational data, a. Cell type, g. Writing, g. Supplemental text writing, and i. Principal. 2018. Single-cell transcriptomics of 20 mouse organs creates a Tabula Muris. *Nature*. 562:367-372.

Tange, O. 2018. GNU Parallel 2018. *https://doi.org/10.5281/zenodo.1146014*.

Terry, E.E., X. Zhang, C. Hoffmann, L.D. Hughes, S.A. Lewis, J. Li, M.J. Wallace, L.A. Riley, C.M. Douglas, M.A. Gutierrez-Monreal, N.F. Lahens, M.C. Gong, F. Andrade, K.A. Esser, and M.E. Hughes. 2018. Transcriptional profiling reveals extraordinary diversity among skeletal muscle tissues. *eLife*. 7:e34613.

Wulf, M.A., A. Senatore, and A. Aguzzi. 2017. The biological function of the cellular prion protein: an update. *BMC Biol*. 15:34.

Yu, G.C., L.G. Wang, Y.Y. Han, and Q.Y. He. 2012. clusterProfiler: an R Package for Comparing Biological Themes Among Gene Clusters. *Omics*. 16:284-287.

Zerr, I., M. Schmitz, A. Karch, A. Villar-Piqué, E. Kanata, E. Golanska, D. Díaz-Lucena, A. Karsanidou, P. Hermann, and T. Knipper. 2018. Cerebrospinal fluid neurofilament light levels in neurodegenerative dementia: evaluation of diagnostic accuracy in the differential diagnosis of prion diseases. *Alzheimer's & Dementia*. 14:751-763.

Materials and Methods.

Animals. Animal experiments were approved by the Veterinary Office of the Canton Zurich (permit numbers ZH41/2012, ZH90/2013, ZH040/15, ZH243/15) and carried out in compliance with the Swiss Animal Protection Law. Animal discomfort and suffering was minimized as much as possible and individual housing was avoided. Prion-inoculated and control-injected mice were regularly monitored for the development of clinical signs, according to well-established procedures using humane termination criteria. Intracerebral injections and transcardiac perfusions were performed in deeply anesthetized mice. Habituation periods before the experiment began were included. Male C57BL/6J mice were obtained from Charles River, Germany. Mice were housed in a conventional sanitary facility and monitored for the presence of all viral, parasitic, and bacterial species listed in the Federation of European Laboratory Animal Associations (FELASA). The facility was tested positive for Murine Norovirus and Helicobacter spp. The mice were housed in IVC type II long cages and up to five animals were housed in the same cage which were staffed with individual apartments. Mice had unrestricted access to sterilized drinking water and were fed *ad libitum* a pelleted mouse diet. The light/dark cycle consisted of 12/12 h with artificial light. The temperature in the room was 21 ± 1 °C with a relative humidity of 50 ± 5%. Air pressure was regulated at 50 Pa, with 15 complete changes of filtered air per hour by a HEPA filter.

Prion inoculations and processing of tissue samples. Animals, prion inoculation and necropsy procedures are identical to those described in (Sorce et al., 2020). C57BL/6J male mice were inoculated in the right hemisphere with either 30 µl of passage 6 of Rocky Mountain Laboratory (RML6), or 22L, or ME7 strain mouse-adapted scrapie prions containing 9.02 LD_{50} of infectious units per ml in 10% w/v homogenate. Non-infectious brain homogenate (NBH) from CD1 mice was used as a negative control. Mice were assigned randomly to experimental groups. Animals were monitored at least thrice per week, after the clinical onset of prion disease, they were monitored daily, and prion-inoculated mice were terminated upon evident signs of terminal disease. NBH-inoculated mice were sacrificed 13 days after the termination of the last prion-inoculated mice. Whole blood, spleen and muscle were dissected, snap-frozen in liquid N_2 and stored at -80 °C prior to sequence library generation.

Processing of AD, DLB and ALS tissue samples. Double-transgenic APP/PS1 mice (n = 3; 8 months of age) were used as AD mouse models from which we have collected hindlimb skeletal muscles. For the DLB mouse model, hindlimb skeletal muscles of transgenic A53T synuclein mutant mice lines were kindly provided by Dr. Noain Daniela's

group (Department of Neurology, University Hospital Zurich; n=2, 8 months of age) and by Dr. Ruiqing Ni's group (Institute for Biomedical Engineering, University Hospital Zurich; n=1, 8 months of age). Non-transgenic C57BL/6J male littermates (n = 3, 8 month old) were used as controls. All mice were housed under a 12-hour light/12-hour dark schedule and had free access to food and water. All animals were euthanized by pentobarbital injection. Skeletal muscles were dissected, snap frozen in liquid N_2 and stored at -80 °C prior to western blot and biochemical analyses.

Differently, skeletal muscle lysates obtained from both wild-type and $SOD1^{G93A}$ transgenic mouse models of ALS were generously provided by Prof. Dr. Musarò, the Principal Investigator leading the neuromuscular research group at the Sapienza University of Rome. To provide a concise overview, wild-type C57BL/6 (WT) and transgenic $SOD1^{G93A}$ mice were utilized for our investigation. The mice were sacrificed at 130–140 days of age, a time point closely aligned with the spontaneous mortality of $SOD1^{G93A}$ mice. Euthanasia was conducted through cervical dislocation to ensure minimal suffering. Immediately following the humane sacrifice, muscle samples were excised for subsequent analysis, with one muscle specimen collected from each animal for testing purposes. Tissue lysates were prepared according to (Dobrowolny et al., 2017).

Preparation of RNA libraries for Mouse sequencing. RNA was extracted from snap-frozen organs by means of the RNeasy Plus Universal Kit (QIAGEN). The quantity and quality of RNA were analyzed with Qubit 1.0 Fluorometer (Life Technologies) and Bioanalyzer 2100 (Agilent Technologies), respectively. For library preparation, we used TruSeq RNA Sample Prep kit v2 (Illumina). We performed poly-A enrichment on 1 µg of total RNA per sample, which was then reverse transcribed into double-stranded cDNA followed by ligation of TruSeq adapters. Sequencing fragments containing TruSeq adapters at both termini were enriched by PCR. Quantity and quality of enriched libraries were analyzed using Qubit (1.0) Fluorometer and Caliper GX LabChip GX (Caliper Life Sciences), which showed a smear corresponding to a mean fragment size of around 260 bp. Libraries were then normalized to 10 nM in Tris-Cl 10 mM, pH 8.5, with 0.1% (v/v) Tween 20. Cluster generation was performed with the TruSeq PE Cluster kit v4-cBot-HS (Illumina), using 2 pM of pooled normalized libraries on the cBOT. Sequencing was performed on Illumina HiSeq 4000 paired-end at 2 × 126 bp using the TruSeq SBS kit v4-HS (Illumina).

Patient samples. We obtained anonymized samples from an approved study sanctioned by the Cantonal Ethics Committee of the Canton of Zurich under approval number #2019-01479. Human skeletal muscle samples of psoas major muscle were collected from patients with a clinical suspicion of Creutzfeldt-Jakob's disease and submitted for an autopsy to the

Swiss National Reference Center for Prion Disease between 2004 - 2011. A detailed description of samples used for RNA extraction and sequencing is given in *Suppl. Table 8*. Sporadic CJD was diagnosed according to criteria described previously (Hill et al., 2003). The experimental protocols involving GLUL's specificity validation test by using human participants adhered strictly to the guidelines set by French regulations. Prior to participation, comprehensive written informed consent was diligently obtained from all individuals, including those who underwent skeletal muscle necropsies for Familial Amyotrophic Lateral Sclerosis (Familial SLA), Fronto-Temporal Dementia with ALS (DFT-SLA), and pure cases of Alzheimer's Disease (AD) and Dementia with Lewy Body (LBD). Human biological samples and associated data were obtained from Tissu-Tumorothèque Est (CRB-HCL, Hospices Civils de Lyon Biobank, BB-0033-00046).

Preparation of RNA libraries for Human sequencing. Firstly, CJD bulk tissues were lysed in TE buffer with the anionic detergent sodium dodecyl sulphate (SDS) and digested at 50°C with 2 mg / ml^{-1} Proteinase K (PK) for 2 hours to eliminate solids and release DNA/RNA from proteins. Although prions are well-known for their relative resistance to PK digestion, prion infectivity largely depends on PK-sensitive oligomers. Indeed, prolonged PK digestion reduces prion titers by a factor of $>10^6$, but residual PK-resistant material may still be infectious. In a second step, TRIzol reagent solution was added to the lysate (it contains Gdn-SCN and phenol, which inactivate RNases and disaggregate prions) and kept overnight at 4°C. Gdn-SCN is a chaotropic salt which rapidly denatures proteins and abolishes the infectivity of prion disease inoculum. At high concentrations, guanidine salts disaggregate PK-resistant PrP^{Sc} fibrils, eliminate PK resistance and abolish PrP^{Sc} conversion, meaning that any PK-resistant material that survived the digestion step would be expected to be inactivated at this stage of the protocol. 0.2 ml of ultrapure phenol:chloroform:isoamyl alcohol (Thermo Fischer Scientific) was added to the samples, followed by strong shaking and incubation at room temperature for 5 mins. Centrifugation step at 12,000 x g for 15 min at 4 °C generated two phases. The aqueous upper phase was transferred to a fresh tube; 0.5 ml of isopropanol and 1 µl of Glycoblue Coprecipitant (Thermo Fisher Scientific) were added. Next, RNA was pelleted for 20 min at 12,000 x g at 4°C and washed twice with 75% ethanol. The RNA pellet was dissolved at 55 °C in 20 µl of free nuclease water.

The quantity and quality of RNA were analyzed with Qubit 1.0 Fluorometer (Life Technologies) and Tapestation 4200 (Agilent Technologies), respectively. The TruSeq stranded RNA protocol (Illumina) was employed for library preparation. In brief, 1 µg of total RNA per sample was poly-A enriched, reverse transcribed into double-stranded cDNA and then ligated with TruSeq adapters. PCR was performed to selectively enrich for fragments containing TruSeq adapters at both ends. The quantity and quality of enriched libraries were

analyzed using Qubit (1.0) Fluorometer and Tapestation 4200. The resulting product is a smear with a mean fragment size of approximately 260 bp. Libraries were then normalized to 10 nM in Tris-Cl 10 mM, pH 8.5, with 0.1% (vol/vol) Tween 20. Cluster generation was performed with the TruSeq PE Cluster kit v4-cBot-HS (Illumina), using 2 pM of pooled normalized libraries on the cBOT. Sequencing was performed on Illumina HiSeq 4000 paired-end at 2 × 126 bp using the TruSeq SBS kit v4-HS (Illumina).

Despite profound RNA degradation, we speculated that moderate RNA degradation might preserve biological information. We then decided to set a RIN ≥ 3 as a minimal threshold for human muscle tissue. 12 out of 28 initially collected samples passed the RIN threshold (*Suppl. Fig. 4a, Suppl. Table 4*) and were further processed. 2 out of 12 samples were subsequently removed because of a high cluster condition variance (upon the quality control of the sequencing) resulting in a final sample size of n = 10 for downstream analysis.

Differential gene expression. We used FASTQC and parallel (Tange, 2018) algorithms for quality control of raw sequencing reads. We clipped low-quality ends as follows: 5' = 3 bases, 3' = 10 bases. Reads were aligned to mm10 for mouse and GRCh38.p13 human reference genome, and transcriptome using STAR v2.3.0e_r291 (Dobin et al., 2013) on cloud computing solution SUSHI of the Functional Genomics Center of Zurich (Hatakeyama et al., 2016). DESeq2 (Love et al., 2014) was used to detect differentially expressed genes based on the following thresholds: (a) $|\log_2\text{-fold change}| > 0.5$ (b) FDR < 0.05. Gene ontology analysis was performed using clusterProfiler for R (Yu et al., 2012).

WGCNA. WGCNA was performed using the WGCNA R package (Langfelder and Horvath, 2008). Outlier genes were identified and removed using the *goodSamplesGenes()* function. Additionally, genes with fewer than 10 counts in over 50% of samples were filtered out. Raw count data was normalized using the variance stabilizing transformation provided by the DESeq2 R package. An adjacency matrix was generated using the *adjacency()* function with default parameters. To meet the criteria for a scale-free network, a soft threshold of 4 was uniformly applied to all networks. Adjacency matrix was transformed into a Topological Overlap Matrix (TOM). Average linkage hierarchical clustering was performed on a dissimilarity matrix (1 – TOM) and subsequently, modules of co-expressed genes were identified using the dynamic cut tree algorithm (*cuttreeDynamic function()*), with a minimum cluster size set to 30. Similar modules were merged based on their module eigengene (ME) correlation. To assess the significance of differences in ME values between tested conditions, a Mann-Whitney U test was conducted. To identify genes with the highest connectivity within modules, Module Membership (MM) was computed as the Pearson correlation coefficient (p-value) between individual gene expression levels and the ME. To

identify hub genes within each module for downstream analysis, we calculated a significance score (SS) based on the p-values obtained from differential expression analysis using DESeq2.

Alternative splicing. SGSeq R package (Goldstein et al., 2016) was employed to find splicing events characterized by two or more splice variants. Exons and splice junction predictions were obtained from BAM files. Prediction of exons and splice junctions was first made for each sample individually. Then the predictions for all samples were merged and we obtained a common set of transcript features. Overlapping exons were disjoint into non-overlapping exon bins and a genome-wide splice graph was compiled based on splice junctions and exon bins. A single value for each variant was produced by adding up the 5' and 3' counts, or, if these represented the same transcript features, by considering the unique value. These counts were then fed to DEXSeq (Anders et al., 2012). We analyzed the differential usage of variants across a single event, instead of quantifying differential usage of exons across a single gene. Events associated with a single variant were discarded. Differential analysis was performed by implementing a sample+exon+condition:exon model in DEXSeq. Differentially expressed isoforms were defined as isoforms changing with FDR < 0.05.

Western blot analysis. To prepare the samples, 1 ml of cell-lysis buffer (20 mM Hepes-KOH, pH 7.4, 150 mM KCl, 5 mM MgCl2, 1% IGEPAL) supplemented with protease inhibitor cocktail (Roche 11873580001) was added to the lysed samples. They were then homogenized twice at 5'000 rpm for 15 seconds using a Precellys24 Sample Homogenizer (LABGENE Scientific SA, BER300P24) and incubated on ice for 20 minutes. The cleared lysates were obtained by centrifugation at 2'000 rcf, 4° C for 10 minutes in an Eppendorf 5417 R tabletop centrifuge. The concentration of whole protein was determined using a BCA assay (Thermo Scientific). The samples were boiled in 4 x LDS (Invitrogen) containing 10 mM DTT at 95°C for 5 minutes. 15 µg of total protein per sample were loaded onto a 4–12% Novex Bis-Tris Gel (Invitrogen) gradient for electrophoresis at 80 V for 15 minutes, followed by constant voltage of 150 V. The PVDF or Nitrocellulose membranes were blocked with 5% Sureblock (LubioScience) in PBS-T (PBS + 0.2% Tween-20) for 1 hour at room temperature. Membranes were then cut into three parts according to the molecular weight. The membrane was divided into three segments for targeted antibody incubation: The upper portion was treated with anti-Vinculin (1:5000, Abcam, ab129002), the middle section with anti-Glutaminase (1:3000, Abcam, ab202027), and the lower segment with anti-Glutamine synthase (1:2000, Abcam, ab176562). This antibody incubation was carried out in PBS-T supplemented with 1% Sureblock, and the membranes were left overnight at 4°C to facilitate optimal binding. They were washed thrice with PBS-T for 10 minutes. The membranes were

incubated with secondary antibodies conjugated to horseradish peroxidase (HRP-tagged goat anti-rabbit IgG (H+L), 1:3000, 111.035.045, Jackson ImmunoResearch) for 1 hour at room temperature. The membranes were washed thrice with PBS-T for 10 minutes and developed using a Classico chemiluminescence substrate system (Millipore). The signal was detected using a LAS-3000 Luminescent Image Analyzer (Fujifilm) and analyzed with ImageJ software.

Biochemical analysis. The concentration of glutamine and glutamate in skeletal muscle was measured using the Merck Glutamine Assay Kit (Catalog Number MAK438). To prepare the lysates, a total of 600 µg of total protein was utilized. In each standard and sample well, 80 µL of working reagent was added to determine the glutamine concentration. To measure glutamate concentration, samples were also prepared with 80 µL of blank working reagent. The 96-well plate was incubated at 37°C for 40 minutes. Absorbance values were recorded at 450 nm using a microplate reader. The concentrations of glutamine and glutamate were determined by comparing the absorbance of the samples to a standard curve generated from known concentrations of glutamine and glutamate. The results were expressed as µM/ml.

Data availability. Raw sequencing data as well as processed data from this manuscript is available freely via GEO accession number GSE210128.

Code availability. Code to reproduce results generated in this manuscript will be available upon publication at https://github.com/marusakod/RML_extraneural_organs.

Author's contributions. DC performed CJD's RNA extraction, sample preparation and analyses, performed all the experimental validations on both animal models and human samples and wrote and reviewed the manuscript. MK analyzed the sequencing data, conceptualized, and developed the shiny app, wrote, and critically reviewed the manuscript. KF analyzed and visualized initial sequencing data, acquired funding, and critically reviewed the manuscript. SS and MN conceived the study. SS, MN, and JB performed an initial analysis of the data, extracted RNA, prepared the sequencing library in cooperation with the Functional Genomics Center Zurich of the ETH Zurich and the University of Zurich, supervised personnel, and critically reviewed the original manuscript. PS bred the animals, performed inoculations, clinical scoring, harvested organs and was responsible for other important tasks related to animal husbandry. SS performed human-related samples validation and critically reviewed the original manuscript. NS made the final diagnosis of DLB, AD and ALS individuals, and performed skeletal muscle biopsies. CS conceived the study, performed initial data analysis, supervised personnel, and reviewed the original manuscript. AA conceived the study, provided animals, personnel and IT resources,

supervised personnel, provided advice on experiments, coordinated the project, acquired funds, wrote parts of the manuscript, and critically reviewed the final manuscript version.

Acknowledgements. KF is a Visiting Faculty Program Fellow at the Department of Molecular Neuroscience, Weizmann Institute of Science, hosted by Prof. Eran Hornstein, and receives unrestricted funding from the Benoziyo Endowment Fund for the Advancement of Science and Swiss Society of Friends of the Weizmann Institute of Science. AA is supported by an Advanced Grant of the European Research Council (ERC, No. 250356), a Distinguished Scientist Award of the Nomis Foundation, grants from the GELU foundation, the Swiss National Foundation (SNF, including a Sinergia grant, #179040, 183563, 207872), and the Swiss Initiative in Systems Biology, SystemsX.ch (PrionX, Synucleix). The authors are grateful to Martina Cerisoli, Nicola Conneely, Marigona Imeri, and Mirzet Delic for support, assistance in laboratory investigations and animal husbandry. The authors acknowledge the Functional Genomics Center Zurich of the ETH Zurich, and Next Generation Sequencing Platform of University of Bern for preparing sequencing libraries, RNA sequencing, quality control and technical support of mouse and human studies, Prof. Eli Eisenberg (Raymond and Beverly Sackler School of Physics and Astronomy and Sagol School of Neuroscience, Tel Aviv University, Tel Aviv, Israel) for help with RNA editing analyses. The authors extend their gratitude to Prof. Musarò Dr. Gabriella Dorbowolny and Dr. Gaia Laurenzi (La Sapienza University), for providing $SOD1^{G93A}$ muscle lysates. Appreciation is also extended to Dr. Daniela Noain, Ines Antunes dos Santos Dias and Irena Barbaric (Department of Neurology, University of Zurich) for their kind contribution of DLB hindlimb skeletal muscles and Dr. Ruiqing Ni's group and Benjamin Francois Combes (Institute for Biomedical Engineering, University of Zurich) for providing DLB hindlimb skeletal muscles. We acknowledge the Tissu-Tumorotheque Est (CRB HCL, HCL's biobank) for providing the human biological samples (AD, DLB, ALS, FTD) used in this study. The funders of the study had no role in study design, data collection, data analysis, data interpretation, or writing of the report. The corresponding author had full access to all the data in the study and had final responsibility for the decision to submit for publication.

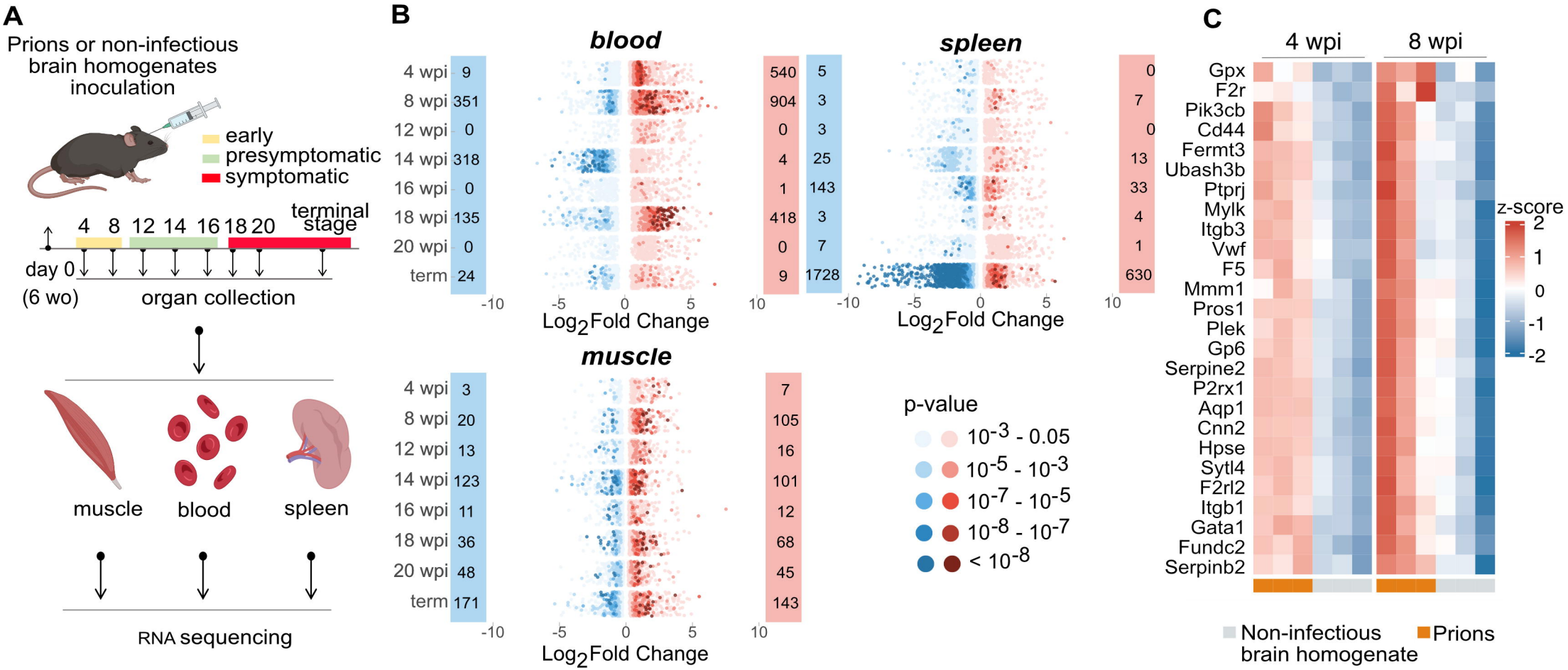
A
Prions or non-infectious brain homogenates inoculation
early
presymptomatic
symptomatic
4 8 12 14 16 18 20
terminal stage
day 0
(6 wo)
organ collection
muscle
blood
spleen
RNA sequencing
B
blood
4 wpi 9
8 wpi 351
12 wpi 0
14 wpi 318
16 wpi 0
18 wpi 135
20 wpi 0
term 24
-10
-5 0 5
Log2Fold Change
540 5
904 3
0 3
4 25
1 143
418 3
0 7
9 1728
10
-10
-5 0 5
Log2Fold Change
spleen
0
7
0
13
33
4
1
630
10
muscle
4 wpi 3
8 wpi 20
12 wpi 13
14 wpi 123
16 wpi 11
18 wpi 36
20 wpi 48
term 171
-10
-5 0 5
Log2Fold Change
7
105
16
101
12
68
45
143
10
p-value
10-3 - 0.05
10-5 - 10-3
10-7 - 10-5
10-8 - 10-7
< 10-8
C
4 wpi
8 wpi
Gpx
F2r
Pik3cb
Cd44
Fermt3
Ubash3b
Ptprj
Mylk
Itgb3
Vwf
F5
Mmm1
Pros1
Plek
Gp6
Serpine2
P2rx1
Aqp1
Cnn2
Hpse
Sytl4
F2rl2
Itgb1
Gata1
Fundc2
Serpinb2
z-score
2
1
0
-1
-2
Non-infectious brain homogenate
Prions

Sup Fig 5a

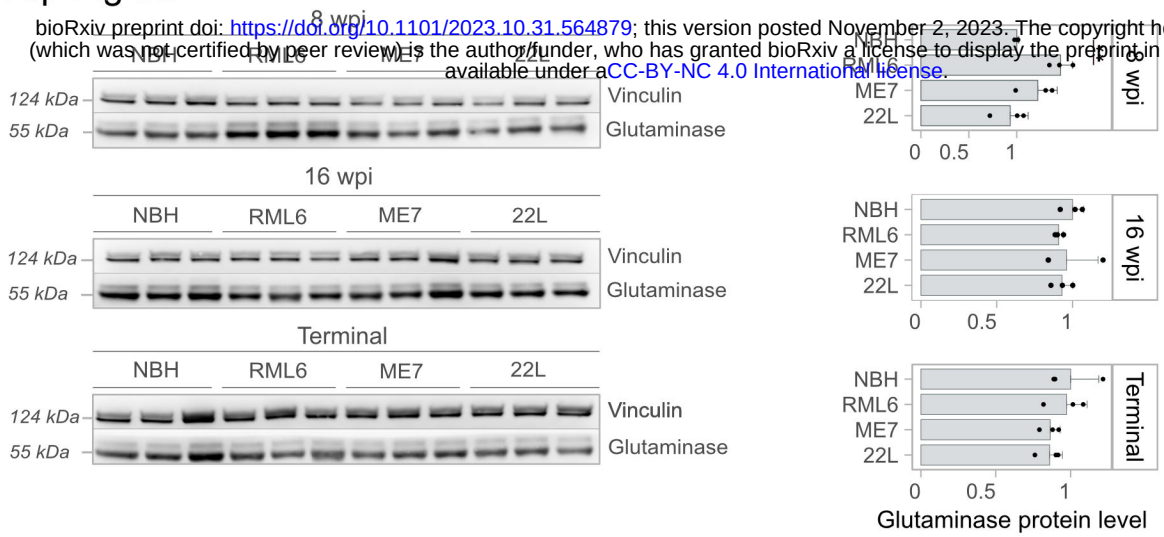

Sup Fig 5b

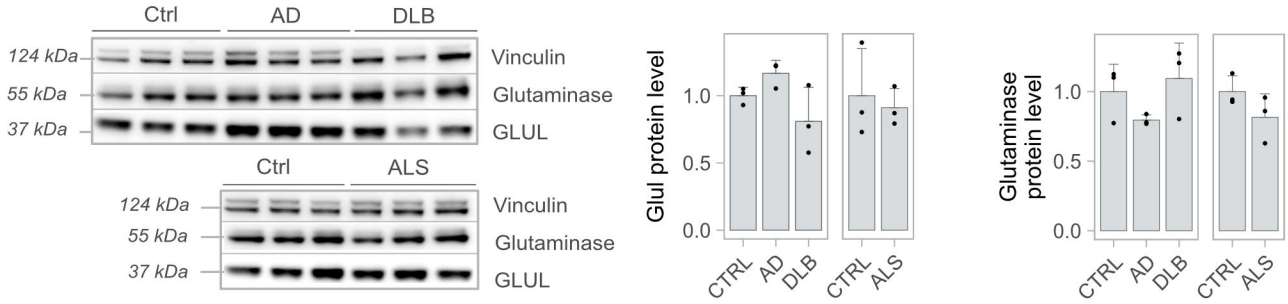

Sup Fig 5c

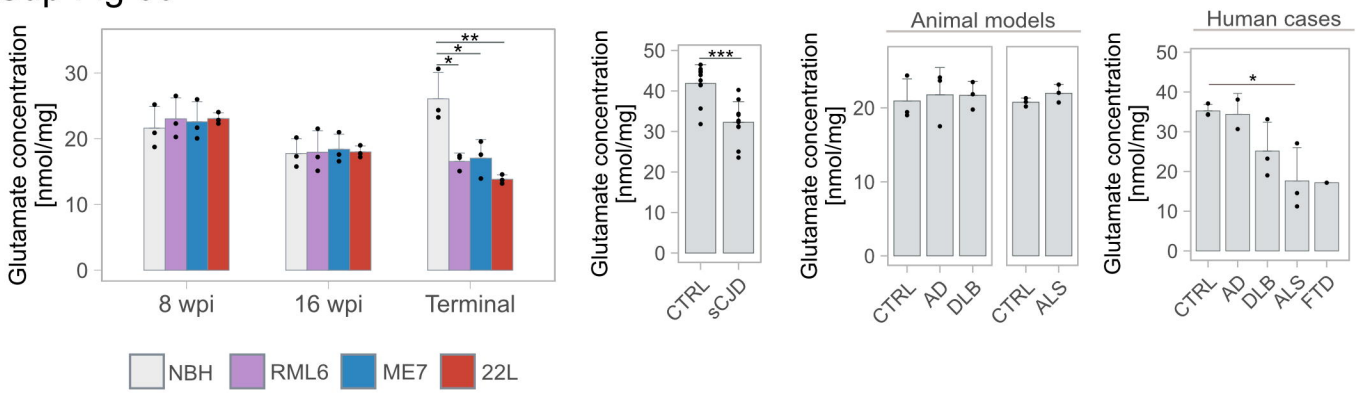

Sup Fig 5d

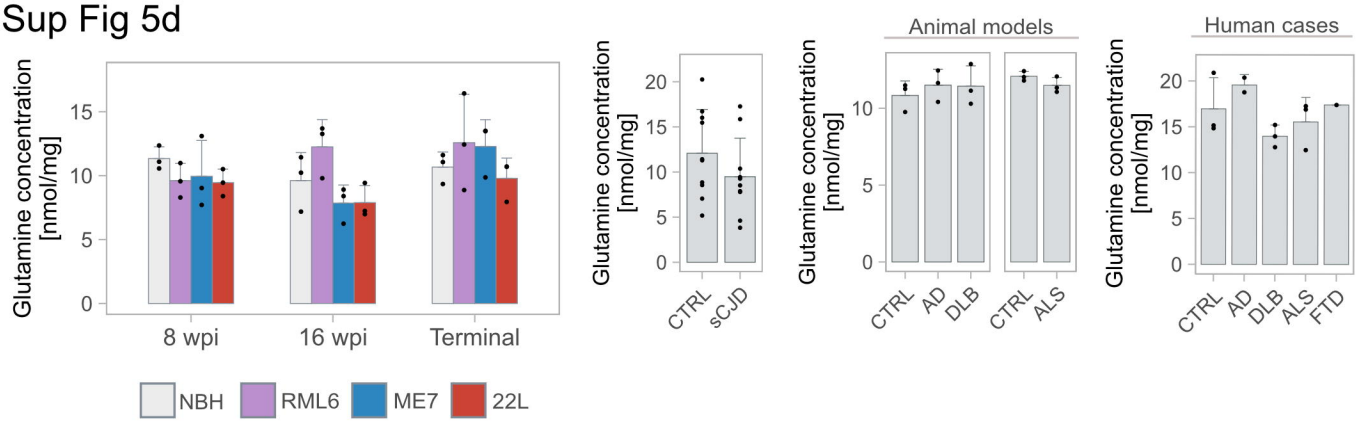

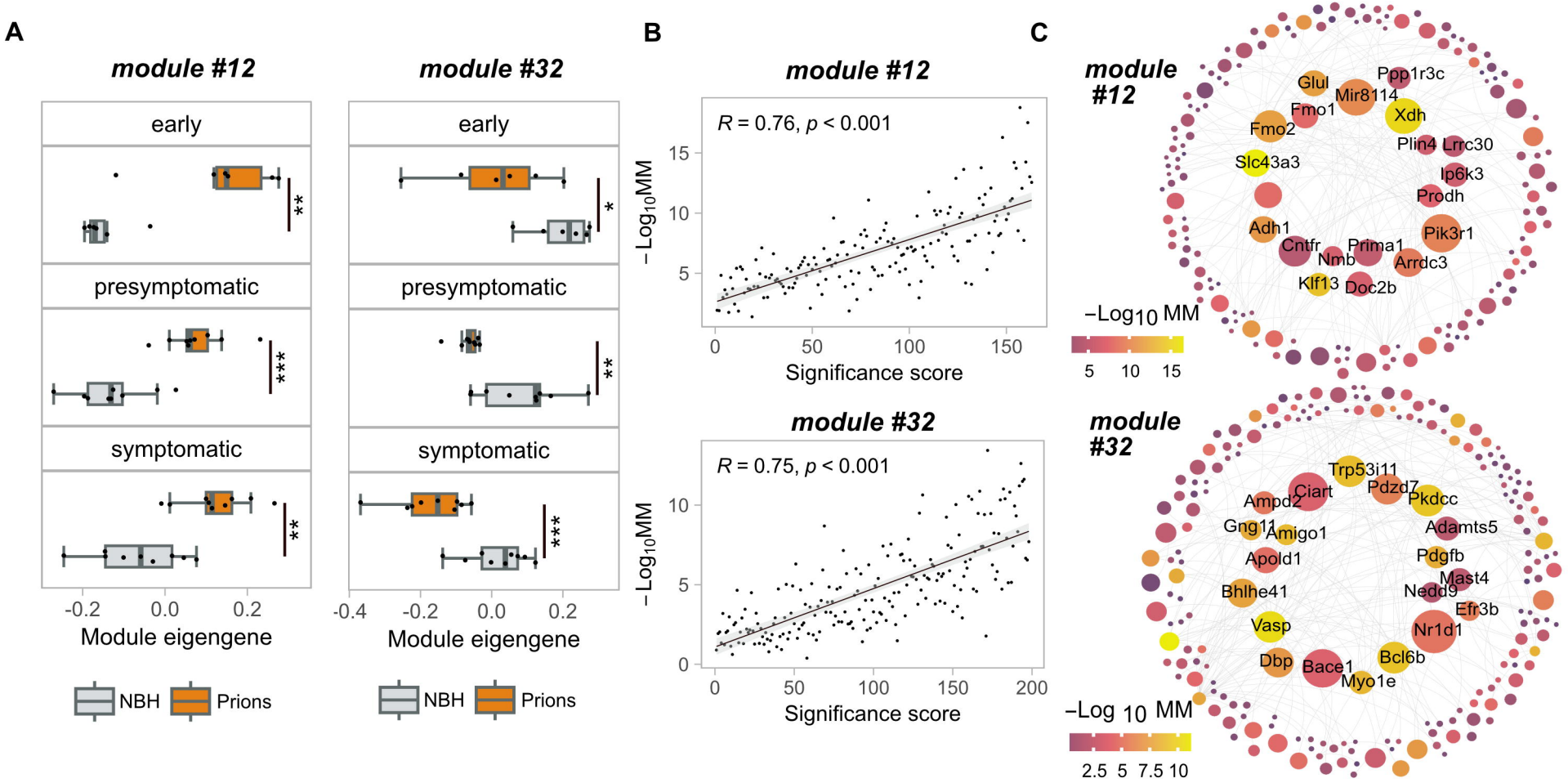
A
module #12
module #32
early
presymptomatic
symptomatic
**
*
***
**
***
-0.2
0.0
0.2
-0.4
-0.2
0.0
0.2
Module eigengene
Module eigengene
NBH
Prions
NBH
Prions
B
module #12
R = 0.76, p < 0.001
−Log10MM
Significance score
module #32
R = 0.75, p < 0.001
−Log10MM
Significance score
C
module #12
Glul
Ppp1r3c
Mir8114
Fmo1
Xdh
Fmo2
Plin4
Lrrc30
Slc43a3
Ip6k3
Prodh
Adh1
Pik3r1
Cntfr
Prima1
Nmb
Arrdc3
Klf13
Doc2b
−Log10 MM
module #32
Trp53i11
Ciart
Pdzd7
Ampd2
Pkdcc
Gng11
Amigo1
Adamts5
Apold1
Pdgfb
Mast4
Bhlhe41
Nedd9
Efr3b
Vasp
Nr1d1
Dbp
Bace1
Bcl6b
Myo1e
−Log 10 MM

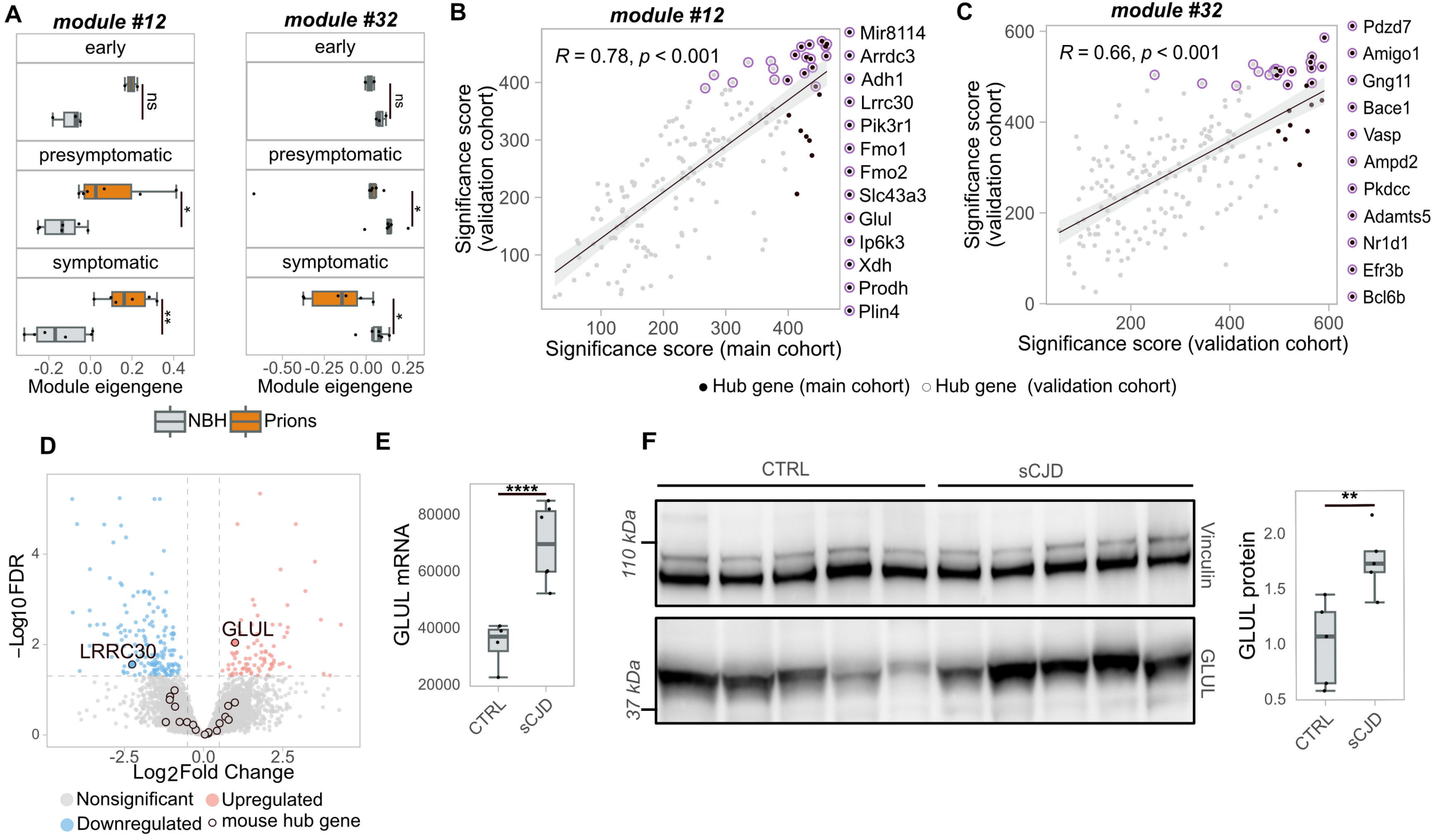
A
module #12
module #32
early
presymptomatic
symptomatic
ns
*
**
-0.2 0.0 0.2 0.4
-0.50 -0.25 0.00 0.25
Module eigengene
NBH
Prions
B
module #12
R = 0.78, p < 0.001
Significance score (validation cohort)
Significance score (main cohort)
Mir8114
Arrdc3
Adh1
Lrrc30
Pik3r1
Fmo1
Fmo2
Slc43a3
Glul
Ip6k3
Xdh
Prodh
Plin4
C
module #32
R = 0.66, p < 0.001
Pdzd7
Amigo1
Gng11
Bace1
Vasp
Ampd2
Pkdcc
Adamts5
Nr1d1
Efr3b
Bcl6b
● Hub gene (main cohort) ○ Hub gene (validation cohort)
D
−Log10 FDR
Log2Fold Change
LRRC30
GLUL
Nonsignificant
Upregulated
Downregulated
mouse hub gene
E
GLUL mRNA
****
CTRL
sCJD
F
CTRL
sCJD
110 kDa
37 kDa
Vinculin
GLUL
GLUL protein
**

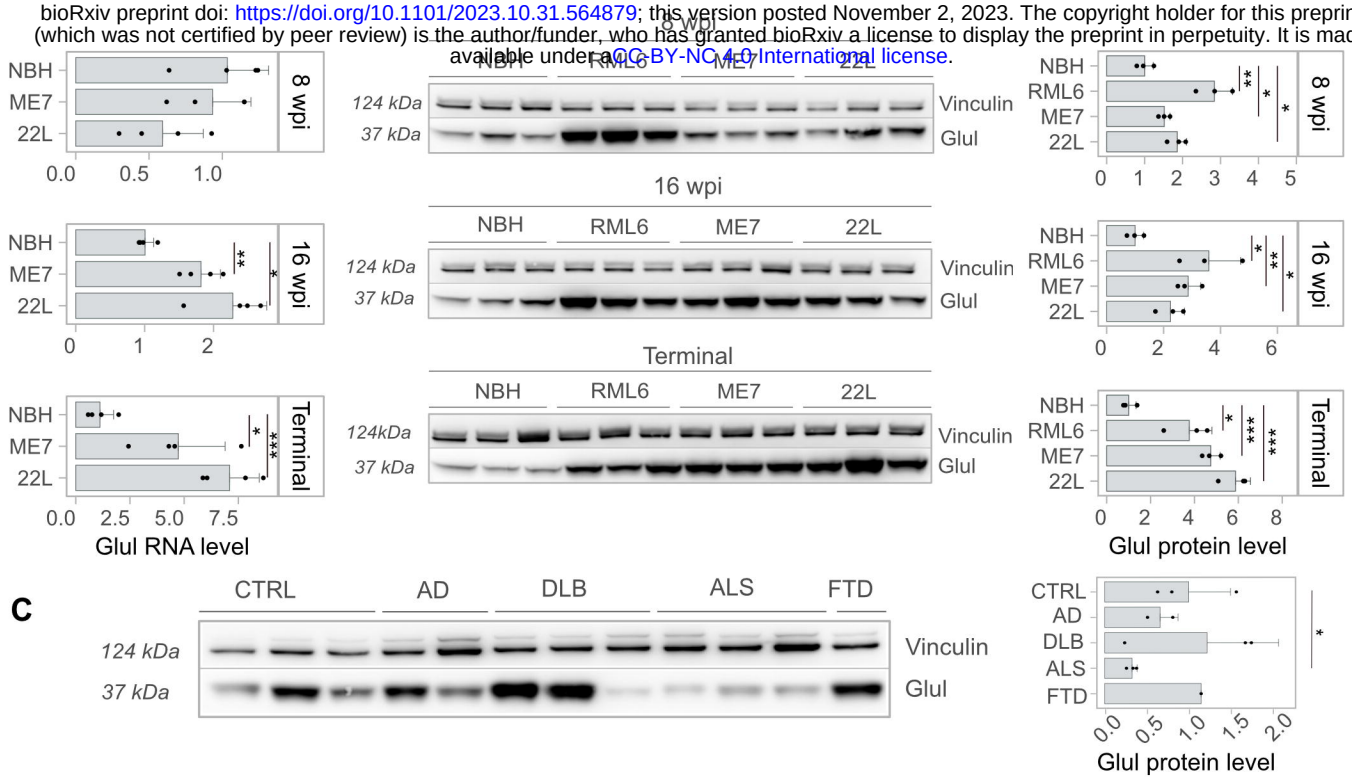

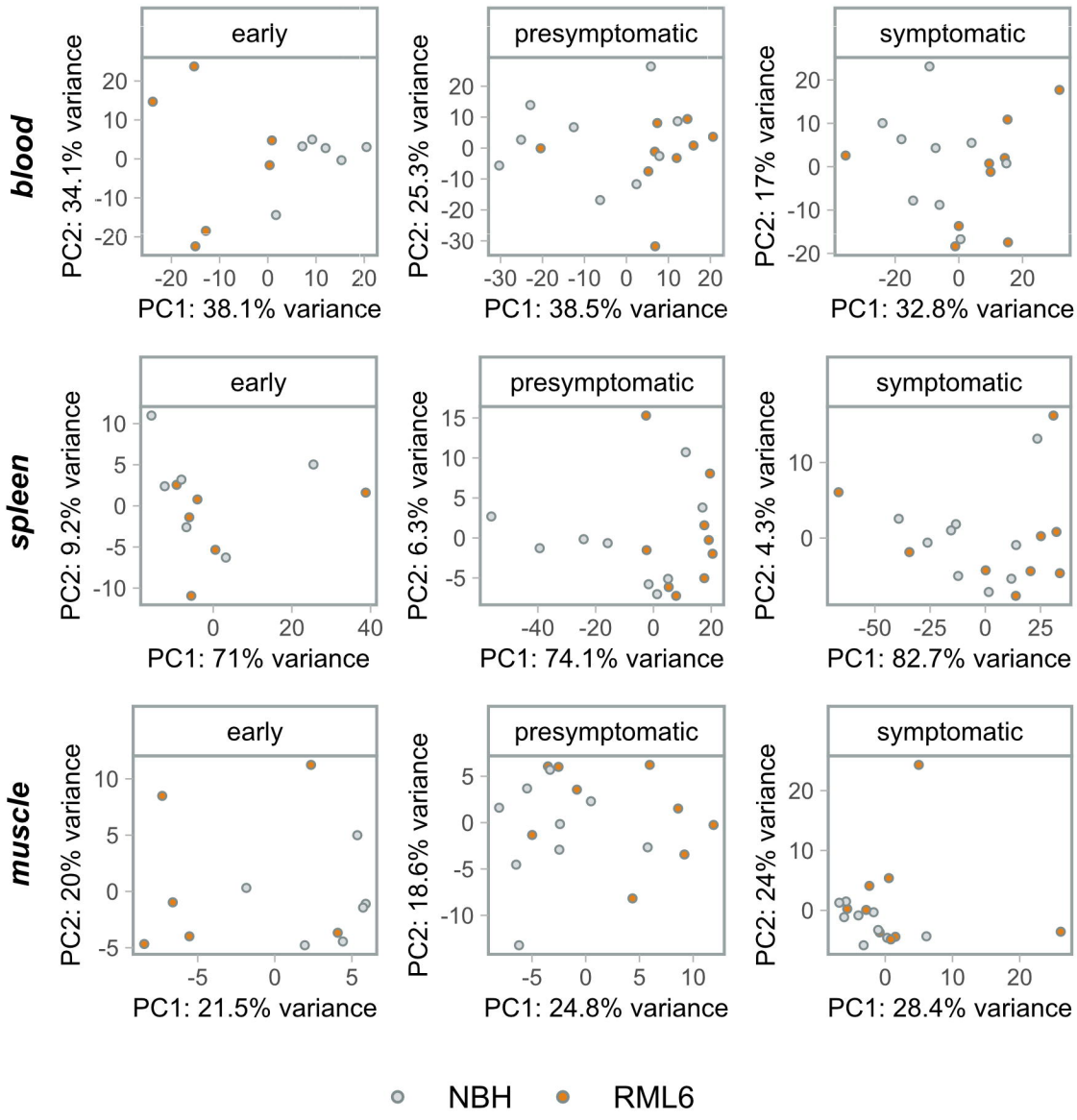

Sup Fig 2a

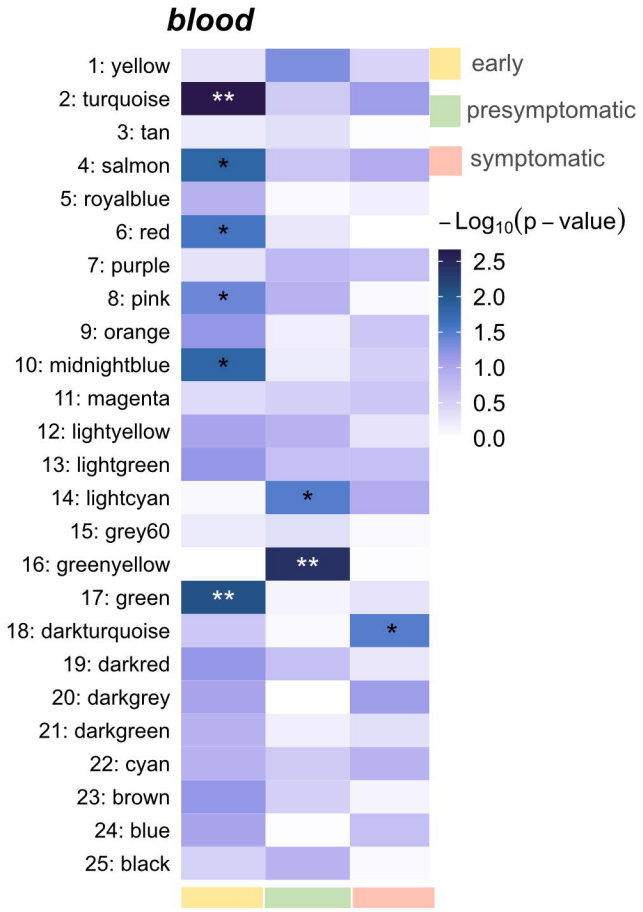

Sup Fig 2b

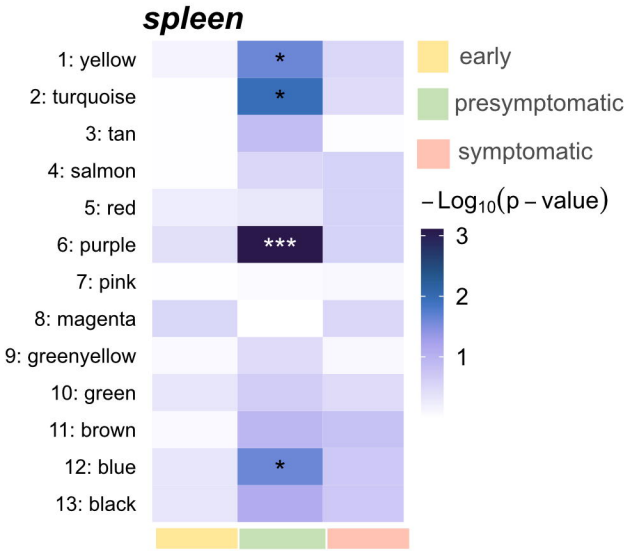

Sup Fig 2c

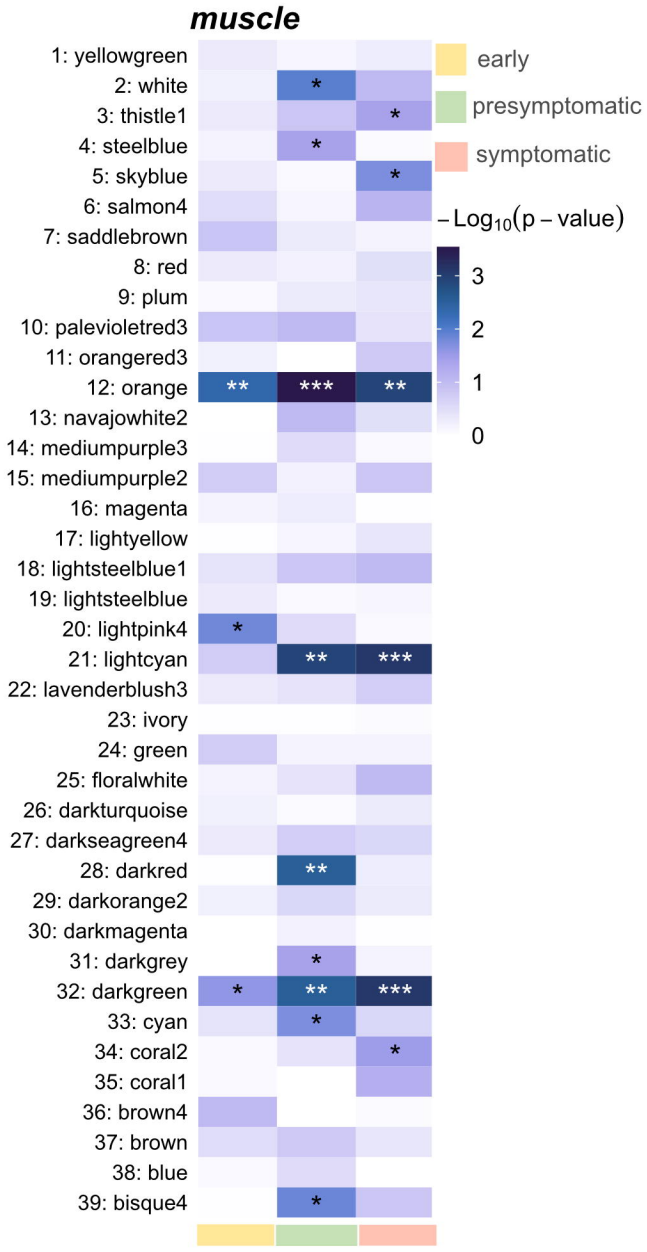

Sup Fig 3a

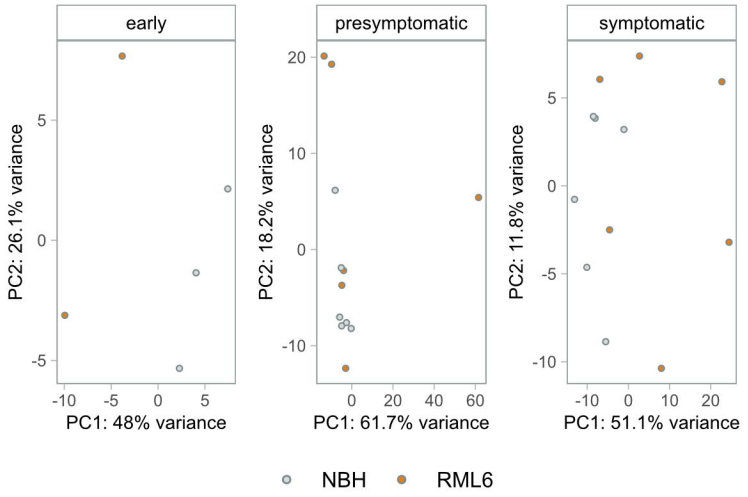

Sup Fig 3b

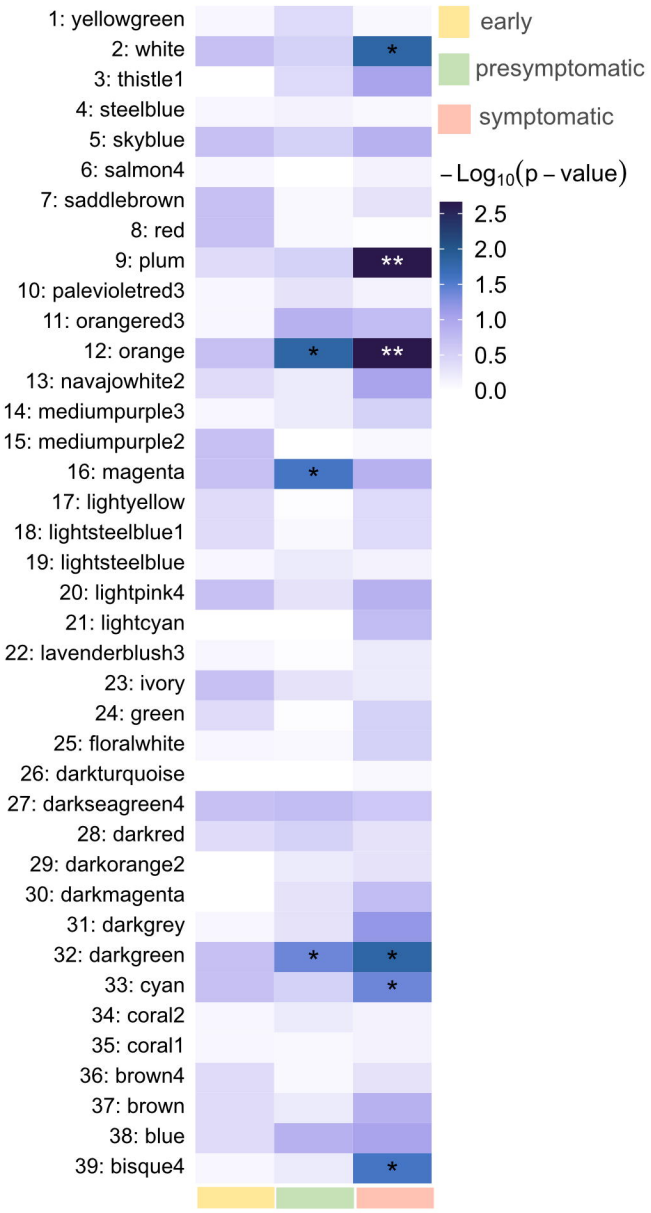

Sup Fig 3c

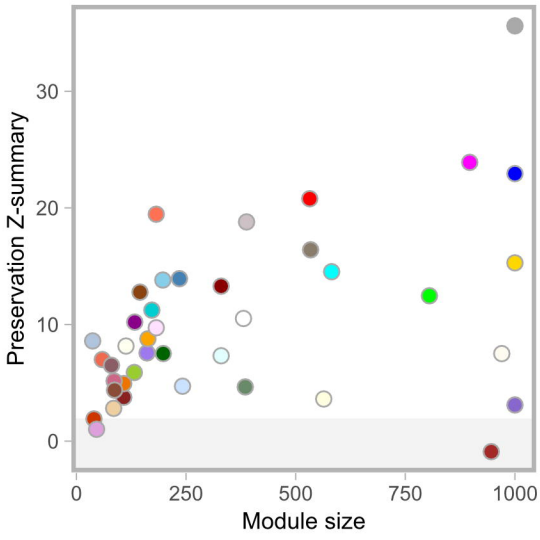

Sup Fig 4a

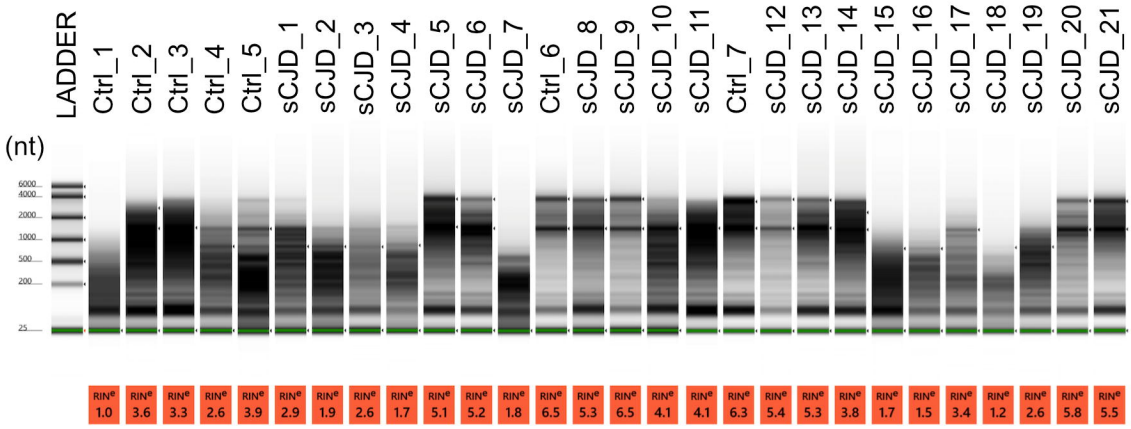

Sup Fig 4b

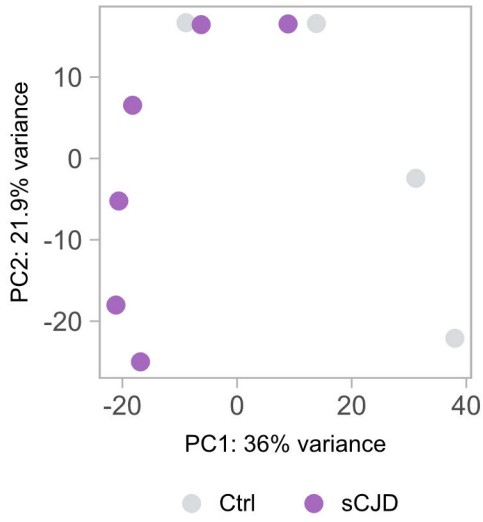

Sup Fig 4c